The assembly of the *Drosophila* mushroom body circuit and its regulation by Semaphorin 1a

Chen-Han Lin[1,2] and Suewei Lin[1,2,#]

[1]Institute of Molecular Biology, Academia Sinica, Taipei 115, Taiwan
[2]Department of Life Sciences and Institute of Genome Sciences, National Yang-Ming University, Taipei 112, Taiwan

[#]Correspondence: sueweilin@gate.sinica.edu.tw

Summary

The *Drosophila* mushroom body (MB) is a learning and memory center in the fly brain. It is the most extensively studied brain structure in insects, but we know little about the molecular and cellular mechanisms underlying the assembly of its neural circuit. The MB is composed of around 2200 intrinsic Kenyon cells (KCs), whose axons are bundled to form multiple MB lobes. The MB lobes are innervated by large number of extrinsic neurons. 20 types of dopaminergic neurons (DANs) and 21 types of MB output neurons (MBONs) have been identified. Each type of these extrinsic neurons innervates specific compartments or zones in the MB lobes. Here, we characterize the assembly of the MB circuit and reveal several intriguing features of the process. The DANs and MBONs innervate the zones in the MB vertical lobes in specific sequential orders. In some zones the innervation of DAN axons precedes that of the MBON dendrites, while the opposite is true in other zones. The innervations of MBONs and DANs are largely independent of each other. Removing one type of extrinsic neurons during early development has minimal effect on the MB lobe innervations of other extrinsic neurons. However, the KC axons are absolutely required for the zonal elaboration of the DAN axons and the MBON dendrites. There are also competitions between MB lobe zones for some MBONs, so when the cognate zones for these MBONs are missing, their dendrites are misdirected to some other zones. Finally, we identified Semaphorin 1a (Sema1a) as a crucial guidance molecule for MBON dendrites to innervate specific MB lobe zones. Ectopic expression of Sema1a in some DANs is sufficient to re-direct their dendrites to those zones, demonstrating a possibility to rewire the MB circuit. Taken together, our work provides an initial characterization of the cellular and molecular mechanisms underlying MB circuit assembly.

Introduction

During brain development, large number of neurons are precisely assembled in a three-dimensional space to form functional networks that ultimately give rise to complex behavior. The assembly process is regulated by intricate cellular and molecular mechanisms. Malfunction of these mechanisms could lead to severe behavioral disorders or even death. Since Roger Sperry proposed his famous chemoaffinity hypothesis, postulating that the precise wiring of the nervous system is established by specific chemical affinities generated from individual neurons, a large number of guidance molecules and principles governing neural circuit development has been discovered (Chédotal and Richards, 2010; Dickson and Zou, 2010; Hong and Luo, 2014; Kolodkin and Tessier-Lavigne, 2011; Sanes and Yamagata, 2009; SPERRY, 1963). However, our understanding of neural circuit assembly remains profoundly insufficient and still unable to explain fully the mechanisms underpinning the wiring process of any neural circuit. Furthermore, given the remarkably diverse cell types and circuit configurations in the brain, additional guiding strategies and molecules must await discovery.

The genetically tractable and sufficiently complex nervous system of the fruit fly *Drosophila* has been a powerhouse for studying neural development. Many important guidance molecular and neural circuit organizing principles are first discovered in the fly (Evans, 2016; Hong and Luo, 2014; Kolodkin and Tessier-Lavigne, 2011; Plazaola-Sasieta et al., 2017; Tessier-Lavigne and Goodman, 1996). However, most fly studies focused on the ventral nerve cord, neuromuscular systems, antennal lobes, and optical lobes. The assembly of the central brain circuits is largely unexplored.

The *Drosophila* mushroom body (MB) is a multi-lobe structure at the center of the fly brain. It is a computational center mediating learning and memory (de Belle and Heisenberg, 1994; Heisenberg, 2003), sleep (Joiner et al., 2006; Pitman et al., 2006), and motivated behavior (Krashes et al., 2009; Senapati et al., 2019; Tsao et al., 2018). The MB circuit is composed of three major types of neurons—Kenyon cells (KCs), MB output neurons (MBONs), and dopaminergic neurons (DANs) (Aso et al., 2014). There are around 2200 KCs in each brain hemisphere. They are the intrinsic MB neurons whose axonal bundles form five MB lobes with α and α′ lobes extending vertically, while β, β′ and γ lobe projecting horizontally. The MB lobes are innervated by the dendrites of ~34 MBONs and the axons of around ~130 DANs. Based on their morphology and molecular markers, 21 types of MBONs and 20 types of DANs have been identified. Each type of MBONs or DANs extends its dendrites or axons, respectively, into specific compartments or zones in the MB lobes. Together, MBONs and DANs subdivide the MB lobes into 15 distinct zones. Most of MBONs and DANs innervate only 1 to 2 zones. Given that the MB lobes are bundles of continuous axonal processes, that each type of MBONs and DANs synapses onto specific domain of the lobes represents an elaborated form of subcellular targeting, a process yet well understood.

The development of the MB has been extensively studied, but mostly focused on the KCs. KCs can be classified into three major types: γ, α′β′, and αβ. They are sequentially produced from four neuroblasts during development (Lee et al., 1999). Several molecular mechanisms have been identified to govern the specification of KC cell fates (Liu et al., 2019, 2015; Marchetti and Tavosanis, 2017; Zhu et al., 2006). The targeting and pruning of the KC axons are also well characterized (Awasaki and Ito, 2004; Boulanger et al., 2011; Boyle et al., 2006; Lee et al., 2000; Lin et al., 2009; Ng et al., 2002; Rabinovich et al., 2016; Shimizu et al., 2011; Shin and DiAntonio, 2011; Smith-Trunova et al., 2015; Wang et al., 2002; Yu et al., 2013; Zwarts et al., 2016). In contrast, much less is known about the development of MBONs and DANs and how they are assembled into the MB circuit. To fill this gap, we first characterized the targeting of MBON dendrites and DAN axons to the MB vertical lobes during the pupal stage when the adult MB circuit is assembled. We then used ablation experiments to probe the requirement of MBONs, DANs, and KCs in the assembly of the MB circuit.

86 Finally, we identified that *semaphorin 1a* (*sema1a*), a classical guidance molecule (Kolodkin et al.,
87 1993), expressing in some MBONs is critical for their dendritic targeting to specific MB lobe zones,
88 and ectopic expression of *sema1a* in some DANs is sufficient to re-direct their dendrites to these
89 zones. Our work provides the first characterization of the assembly of the MB circuit and reveals a
90 role of *sema1a* in the dendritic targeting of MBONs.
91

Results

The innervation timings of DAN axons and MOBN dendrites in the MB vertical lobes

To investigate the assembly of the MB circuits, we first aimed to identify GAL4 lines that label individual types of DANs and MBONs throughout their morphogenesis. We focused on the MBONs and DANs that innervate the MB vertical lobes because their types and number are fewer than those innervating the horizontal lobes (Aso et al., 2014). In all the GAL4 lines we have checked, *MB058B-splitGAL4* and *MB091C-splitGAL4* specifically label PPL1-α′2α2 DANs and MBON-α′2, respectively, throughout their development (**Fig. 1A-L'**). Since PPL1-α′2α2 DANs and MBON-α′2 are the only DANs and MBONs that innervate the α′2 zone (Aso et al., 2014), following the development of these neurons allows us to study the innervation order of DAN axons and MBON dendrites in the same MB lobe zone. We used *MB058B* and *MB091C* to drive the expression of mCD8::GFP in PPL1-α′2α2 DANs and MBON-α′2 and checked their morphologies at various times after puparium formation (APF). The PPL1-α′2α2 DANs begin to touch the MB lobes at 18 h APF, starting from the lateral surface of the α′2 zone (**Fig. 1A-A'**). At 24 h APF, the innervation became obvious with axons extending ventrally along the interfaces between α′ and α lobes (**Fig. 1B-B' and M-M''**). Dense zonal innervation of the PPL1-α′2α2 axons were observed at 36 h APF (**Fig. 1D-D'**). The dendritic targeting of MBON-α′2 in the α′2 zone occurs later. At 42 h APF, MBON-α′2 dendrites only began to touch the medial surface of the α′2 zone and dense zonal elaboration of the MBON-α′2 dendrites were seen at 48 h APF (**Fig. 1K-K'**). Therefore, in the α′2 zone, the DAN axons innervate the MB lobes earlier than the MBON dendrites.

Interestingly, it seems that not in all MB lobe zones the DAN axons precede the MBON dendrites. In the α′3 zone, the MBON-α′3 dendrites likely innervate the MB lobes earlier than the PPL1-α′3 axons. The innervation of MBON-α′3 dendrites (labeled with *MB027B-splitGAL4*) was observed at 6 h APF, much earlier than that of their neighboring MBON-α′2 (**Fig. S1**). However, when we labeled the DANs with antibodies against tyrosine hydroxylase (TH), an enzyme required for the synthesis of dopamine (Neckameyer and Quinn, 1989), we found that the expression of TH is sequentially turned on, beginning from the base of the vertical lobes and finishing at the tips of the α and α′ lobes (**Fig. S2**). The expression of TH in the α′3 zone only became obvious at 54 h APF, the latest among all vertical compartments. Because the anti-TH signal was first seen in the α′2 and α2 zones at 24 h APF, the expression of TH appears to correlate the innervation of the DANs (**Fig. 1B-B' and Fig. S2**). These data suggest that MBON dendrites precede DAN axons in the α′3 zone.

The zonal innervations of DANs and MBONs are independent of each other.

Given that the axons of PPL1-α′2α2 DANs precede the MBON-α′2 dendrites in the α′2 zone, we next examined the possibility that DAN axons provide guidance cues for MBON dendrites. We genetically ablated PPL1-α′2α2 DANs by ectopically expressing apoptotic genes *head involution defective* (*hid*) and *reaper* (*rpr*) (Grether et al., 1995; White et al., 1994) in these neurons using *MB058B-splitGAL4*. In PPL1-α′2α2 DAN-ablated adult brains, no *MB058B*-positive cells were seen, and the α′2 and α2 MB lobe zones were free from anti-TH staining (**Fig. 2A-A' and B-B'**). The ablation of PPL1-α′2α2 DANs occurred early enough in development and all *MB058B*-positive neurites were eliminated before 24h APF, when PPL1-α′2α2 DANs start to innervate the MB lobes in wild-type brains (**Fig. S3**). The TH-negative zones in the PPL1-α′2α2 DAN-ablated brains suggest that axon-axon contacts between neighboring DANs have minimal effect in determining the borders of the zonal elaboration of the DAN axons in the MB lobes. Ablation of PPL1-α′2α2 DANs did not affect the dendritic targeting of the MBON-α′2 (labeled with *R20G03-LexA::P65*-driven *rCD2-RFP*), suggesting that PPL1-α′2α2

DANs do not provide guidance cues for the MBON-α′2 dendrites (**Fig. 2A''-A''' and B''-B'''**). Ablation of PPL1-α′2α2 DANs also had no effect on the dendritic elaboration of MBON-α′3 (labeled with *R53F03-LexA::P65*-driven *rCD2-RFP*) and MBON-γ2α′1 (labeled with *R25D01-LexA::P65*-driven *rCD2-RFP*) in the neighboring zones (**Fig. S4**). Similarly, ablating MBON-α′2 before its dendrites innervate the MB lobes did not influence the zonal elaboration of the MBON-α′3 and MBON-γ2α′1 dendrites (**Figs. 2C-D'' and S5**), indicating that dendritic tiling is not a mechanism that determines the borders between MBON dendrites in the neighboring zones. Therefore, the zonal elaboration of the DAN axons and MBON dendrites is largely independent of each other.

Interestingly, when we ablated MBON-α′3, the morphology of the α′ lobe (labeled by the KC-specific driver *MB247-LexA* and *LexAop-rCD2::RFP*) was altered (**Fig. 3**). The tip of the α′ lobe (i.e. the α′3 zone) became smaller and the α′ lobe appears shorter in adult brains without MBON-α′3 (**Fig. 3A-E**). We followed the development of the MB lobes at different pupal stages in MBON-α′3-ablated brains and found that the growth of the α′ lobe was slower than the wild-type controls (**Figs. S6 and 3F**). This result suggests that the reduced α′3 tip was caused by a developmental defect, not neurodegeneration. The α′3 zone did not completely disappear when MBON-α′3 was ablated, because when we labeled MBON-α′2 with *R20G03-LexA::P65*, its dendrites remained staying clear from the reduced tip of the α′ lobe (**Fig. 3G-H''**). These data suggest the MBON-α′3 dendrites might provide a positive signal to promote the growth of the KC axons. Alternatively, the innervation of the MBON-α′3 dendrites might simply inflate the α′3 zone in wild-type brains. However, the later explanation seems less likely because we did not observe similar reduction of the α′2 zone when MBON-α′2 were ablated (**Fig. 3I**).

The KC axons are essential for the zonal elaborations of the DAN axons

To investigate the role of the KC axons on the axonal and dendritic targeting of the DANs and MBONs, respectively, we took advantage of the *alpha lobe absent* (*ala*) mutant. The *ala* mutant brains have been shown to randomly lose MB vertical lobes or horizontal lobes (Pascual and Préat, 2001; Pascual et al., 2005). We found that in the *ala* mutants that lose MB vertical lobes on one side of the brain, both contralateral and ipsilateral axons of PPL1-α′2α2 wandered around the areas near their missing targets without forming normal zonal elaboration patterns (**Fig. 4A-B''**). The mistargeting of PPL1-α′2α2 axons was 100% correlated with the lobe-missing phenotype (n=9), and thus was not caused by loss of *ala* gene per se but the consequence of lobe-missing. We also examined the PPL1-α′2α2 axons in the *ala* mutant brains at 30 h APF, when obvious zonal innervation of the axons is first observed (**Fig. 1C-C''**). We found that when vertical lobes were absent, the PPL1-α′2α2 axons failed to form a zonal elaboration from the very beginning, and some mistargeted neurites can be found slightly above and posterior to where the α′2 and α2 zones were supposed to locate (**Fig. 4C-D'**). Because these mistargeted axons can still project to places close to their normal targets (**Fig. 4**), the KC axons appear not to provide long-range guidance cues for these axons. Instead, the KC axons may provide local positional cues for the DAN axons to form zonal elaborations. This scenario was further evident when we used multi-color flip-out technique to label PPL1-α′2α2 and PPL1-α′3 DANs in different colors. We found that the primary neurites of these two DANs entered the MB lobes at the similar location (**Fig. S9**). However, PPL1-α′2α2 axons exclusively occupy the α′2 and α2 zones below the entry point, whereas PPL1-α′3 axons specifically cover the α′3 zone above the entry point (**Fig. S8**), suggesting the existence of local cues instructing the direction of zonal elaboration for the DAN axons.

Competition between MB lobe zones for MBON-α′2 dendrites

193 Surprisingly, when the MB vertical lobes were missing, the MBON-α′2 dendrites changed their
194 targets and innervated the β′2p and α′1 zones (**Fig. 5A-B′′**). A previous study shows that in the
195 vertical lobe-missing *ala* mutant MB, about half of the KCs lose their vertical branches and the other
196 half have their vertical branches project horizontally (Pascual et al., 2005). However, the
197 mistargeting of the MBON-α′2 is unlikely caused by the horizontally-projecting KC vertical branches
198 for two reasons. First, the zones innervated by the mistargeted MBON-α′2 dendrites are located at
199 the two ends, not middle, of the β′ lobe. Second, the guidance molecules required for MBON-α′2 to
200 innervate the α′2 zone are different from those required for it to innervate the β′2 and α′1 zones
201 (see below). When we followed the development of the MBON-α′2 dendrites in the absence of their
202 normal target, we found that they never formed zonal elaboration near the missing target and
203 started to innervate the β′2p and α′1 zones at around 72 h APF (**Fig. 5C-E′**). Taken together, these
204 results indicate that there are competing guidance cues from multiple MB lobe zones for the MBON-
205 α′2 dendrites. When the stronger guidance cues from the α′2 zones are missing, the MBON-α′2
206 dendrites are attracted to other zones.
207
208
209 **Overexpression of *sema1a* in DANs mistargets their dendrites to specific MB lobe zones**
210
211 During the course to identify genes controlling the MB circuit assembly, we found that when *sema1a*
212 was overexpressed in PPL1-α′2α2 DANs, their dendrites that normally elaborate loosely behind the
213 MB vertical lobes (**Fig. 6A-A′′**) became to innervate the β′2p, α′1, and α′3 zones (**Fig. 6B-B′′**). We
214 confirmed these misguided neurites are dendrites by labeling PPL1-α′2α2 with DenMark and dSyd1-
215 GFP (**Fig. 6E-E′′**). The dSyd-1-GFP labeled axons were not affected by the overexpression of *sema1a*.
216 Sema1a can function as ligand or receptor in different developmental contexts (Cafferty et al., 2006;
217 Godenschwege et al., 2002; Komiyama et al., 2007; Winberg et al., 1998). We found that
218 overexpression of *sema1a* without its intracellular domain (Sema1a-mEC-5xmyc and Sema1a-
219 mEC.Fc-5xmyc)(Jeong et al., 2012) in PPL1-α′2α2 DANs had no effect on their dendritic targeting (**Fig.
220 6C-C′′**), suggesting that when overexpressed, Sema1a works as a receptor to guide the PPL1-α′2α2
221 dendrites to the MB lobes zones where the ligands for Sema1a are likely produced. Overexpressing
222 *sema1a* in PPL1-γ2α′1 DANs using *MB296B-splitGAL4* also caused mistargeted dendrites, which,
223 however, innervate the β′2mp and β′2a zones (**Fig.6F-I′′**). Interestingly, this manipulation resulted in
224 loss of MB vertical lobes due to an unknown mechanism. It is striking that overexpression of *sema1a*
225 in different DANs leads their dendrites to distinct β′2 zones, suggesting that Sema1a may work with
226 other guidance molecules to determine zonal specificity for different dendrites.
227
228 Overexpression of *sema1a* cannot always outcompete the endogenous dendritic targeting program.
229 This is evident for MBON-α′2, whose overexpression of *sema1a* did not lead to any dendritic
230 targeting phenotype (**Fig. S8**). However, the ectopic innervation of the *sema1a*-overexpressed PPL1-
231 α′2α2 dendrites in the β′2p and α′1 is reminiscent of the mistargeting of the MBON-α′2 dendrites in
232 the absence of MB vertical lobes (**Fig. 5**). Therefore, we tested if *sema1a* is required for the
233 mistargeting of MBON-α′2 in *ala* mutant brains. We knocked down *sema1a* in MBON-α′2 in *ala*
234 mutant flies and found that MBON-α′2 with reduced *sema1a* expression no longer innervated the
235 β′2 and α′1 zones when their normal target was missing (**Fig. 7**). Knockdown of *sema1a*, however,
236 did not affect their dendritic targeting to the α′2 zone in the normal vertical lobes (**Fig. 7**). These
237 results suggest that MBON-α′2 may expresses *sema1a* and a yet identified guidance molecule. In
238 wild-type brains, the unknown guidance molecule outcompetes *sema1a* to lead the MBON-α′2
239 dendrites to the α′2 zone. When the α′2 zone is missing, a *sema1a*-depedent guidance mechanism
240 will take over and bring the dendrites to the β′2 and α′1 zones.
241
242
243 ***Sema1a* is required for dendritic targeting of several MBONs**

The ectopic innervation of *sema1a*-overexpressed PPL1-α′2α2 and PPL1-γ2α′1 dendrites in the β′2, α′1, and α′3 zones prompted us to examine the role of *sema1a* in the dendritic targeting of the MBONs innervating these three zones. We found that RNAi knockdown of *sema1a* in MBON-β2β′2a using *MB399B-splitGAL4* resulted in mistargeting of the dendrites that normally innervate the β′2a zone (**Fig. 8A-D**). Instead of innervating the β′2a zone, these dendrites project upward to regions near the central complex. The MBON-β2β′2a dendrites innervating the β2 zone were minimally affected by *sema1a* knockdown (**Fig. 8A-D**), suggesting that *sema1a* regulates the dendritic targeting of MBON-β2β′2a in a zone-specific manner. Similarly, when *sema1a* was knocked down in MBON-α′3 using *MB027B-splitGAL4*, the MBON-α′3 dendrites failed to concentrate in the α′3 zone but elaborated loosely around the α′3 zone (**Fig. 8E-H**). We confirmed these findings by creating *sema1a* MARCM clones for MBON-β2β′2a (**Fig. 9A-B′**) and MBON-α′3 (**Fig. 9C-D′**). The dendritic targeting defects observed in *sema1a* mutant MBON-β2β′2a and MBON-α′3 are consistent with the phenotypes caused by *sema1a* RNAi knockdown. To confirm that MBON-β2β′2a and MBON-α′3 express *sema1a*, we used *sema1a* Artificial exon that produces V5-tagged Sema1a and LexA::p65 under the control of the endogenous *sema1a* enhancer when a FRT-stop-FRT cassette in the exon is removed by Flipase (FLP) (Pecot et al., 2013). Consistently, V5-tagged Sema1a and LexA::P65 driven by *sema1a* enhancer were detected in MBON-β2β′2a and MBON-α′3 when *MB399C*- and *MB027B-splitGAL4* were respectively used to drive *UAS-FLP* (**Fig. S9**).

MARCM also allows us to test the role of *sema1a* in MBONs in which we do not have GAL4 lines to drive RNAi early enough during their development. In addition to MBON-β2β′2a, the β′2 zone is also innervated by MBON-β′2mp and MBON-γ5β′2a, and the α′1 zone is innervated by MBON-γ2α′1 and MBON-α′1. Dendritic targeting remained normal in *sema1a* MARCM clones for MBON- γ2α′1 and MBON-γ5β′2a (**Fig. S10**). However, *sema1a* MARCM clones for MBON-α′1 exhibited a severe dendritic targeting defect (**Fig. 9E-F′**). We induced clones at 4-8 h after egg laying (AEL) and labeled the MBON-α′1 using *R24H08-GAL4*, which also labels MBON-α′3. Interestingly, all the MBON-α′1 clones were accompanied by MBON-α′3 clones, suggesting that these two neuron types are in the same neuronal lineage. We also observed a dendritic targeting defect in *sema1a* MARCM clones for MBON-β′2mp (**Fig. 9G-H′**). Taken together, these results indicate that *sema1a* is required for dendritic targeting in most MBONs innervating β′2, α′1, and α′3 zones.

Canonical partners of Sema1a are not essential for the targeting of MBON dendrites

Sema2a, Sema2b, and PlexA have been identified as ligands for Sema1a (Sweeney et al., 2011; Yu et al., 2010). To test if these molecules play a role in the targeting of MBON dendrites, we first examined the dendritic innervation patterns of MBON-β2β′2a and MBON-α′3 in flies carrying homozygous mutations in both *sema2a* and *sema2b* genes (*Sema2b*^{f02042}, *sema2a*^{p2})(Sweeney et al., 2011). Although the MB lobe structure is slightly abnormal in these flies, the morphology of MBON-β2β′2a and MBON-α′3 dendrites and their zonal innervations were essentially normal (**Fig. 10A-B′**). Therefore, Sema2a and Sema2b are unlikely the guidance molecules that steer *sema1a*-positive MBON dendrites to specific MB lobe zones. Flies without PlexA activity fail to survive to adulthood. To examine the potential role of PlexA in guiding the MBON dendrites, we took advantage of a weaker *sema1a-RNAi-2* line whose overexpression resulted in mild dendritic targeting defects in MBON-β2β′2a and MBON-α′3 (**Fig. 10C-C′ and E-E′**) and then checked if loss of one *plexA* allele enhances the defects. However, the dendritic targeting defects of MBON-β2β′2a and MBON-α′3 were not enhanced in flies heterozygous for a *plexA* mutant allele, *plexA*^{EY16548} (**Fig. 10C-F′**). We also expressed an *UAS-plexA-RNAi* construct that has been shown to knock down *plexA* effectively (Pecot et al., 2013) in all neurons (*nSyb-GAL4*) or in all gila (*repo-GAL4*). We then examined the dendritic innervation of MBON-β2β′2a (*R12C11-LexA*-driven rCD2-RFP) and MBON-α′3 (*R53F03-LexA*-driven

295 rCD2-RFP) in the MB lobes. However, we did not observe any dendritic targeting phenotype in all
296 cases (**Fig. 10G-N'**). We therefore did not find evidence supporting the involvement of the three
297 known Sema1a ligands in guiding the dendrites of MBONs during the assembly of the MB circuit.
298

Discussion

The MB is the most studied structure in the fly brain. It is conventionally considered as an olfactory learning and memory center in the fly brain (Aso et al., 2014; de Belle and Heisenberg, 1994; Heisenberg, 2003). Recently, it has also been shown to receive other sensory inputs and mediate motivational control of innate behavior (Krashes et al., 2009; Masek and Scott, 2010; Masek et al., 2015; Senapati et al., 2019; Tsao et al., 2018; Vogt et al., 2014, 2016). Almost all the neurons that form the MB circuit have been identified and genetic means to label individual type of these neurons has been developed (Aso et al., 2014). However, our understanding of the assembly process of this important structure is essentially a void. In this study, we provide an initial characterization of this process and reveal several interesting principles.

The most intriguing feature for the organization of the MB circuit is the zonal innervation of the DAN axons and MBON dendrites in the MB lobes. Electron microscopy reconstruction of the MB lobes shows that in each zone, the DAN axons and MBON dendrites form synapses with each other and the KC axons (Takemura et al., 2017). The borders of the zones are clear and there is minimal overlap between DAN axons or MBON dendrites in the neighboring zones. With such a highly organized neural network, one might expect elaborate interactions among the extrinsic neurons. For example, dendritic tiling as observed between dendritic arborization (da) neurons in the fly larvae might be required for the formation of zonal borders (Grueber et al., 2002), and matching between DAN axons and MBON dendrites in the same zone might be important for these neurites to establish proper zonal innervation patterns. However, our results suggest that the targeting and elaboration of the DAN axons and MBON dendrites are largely independent. In the α′2 zone, where the innervation of the DAN axons precedes the MBON dendrites, the ablation of DAN does not affect the zonal elaboration of the MBON dendrites. Also, ablation of one type of DANs or MBONs, the morphologies of the neighboring neurites appear to be normal. Therefore, the size and location of the zonal elaboration of the DAN axons and MBON dendrites might be mainly determined by the interaction between the KC axons and these extrinsic neurons.

The KC axons are apparently essential for the zonal arborization of the DAN axons and MBON dendrites. When their target lobes are absent, the DAN axons stray around the missing target with less exuberant neurite arbors. Therefore, the KC axons appear to promote the growth and arborization of the DAN axons. Do the KC axons also determine the size and border of the zonal arbors? It is still possible that the KCs axons simply provide an anchoring point for the DAN axons and MBON dendrites to grow upon, and the size of their arborization is determined cell-autonomously as an intrinsic property. However, the axonal innervation pattern of the PPL1 DANs argues against the later possibility. The axonal projections of PPL1-α′3 and PPL1-α′2α2 DANs enter the MB vertical lobes at almost the same location, whereas they specifically innervate distinct zones on the opposite sides of the entry point. Therefore, different segments in the KC axons might provide positional cues for the DANs and MBONs, although a direct evidence remains to be sought. What could be the nature of these positional cues if they exist? One possibility is the KC axonal segment in each zone expresses a unique guidance molecule that binds to a receptor on the neurites of the DANs and MBONs projecting to this segment. However, when the target zone of MBON-α′2 is lost, its dendrites turn to innervate β′2, α′1, and α′3 zones. This result suggests that a MBON is capable of reading multiple positional cues. Furthermore, since *sema1a* is required for MBONs to innervate multiple specific MB lobe zones, the positional cues are likely combinatorial.

Sema1a can function as both ligand and receptor (Cafferty et al., 2006; Godenschwege et al., 2002; Komiyama et al., 2007; Winberg et al., 1998). Using *sema1a* transgenes that lack the intracellular domain, we demonstrated that it works as a receptor in MBONs to guide their dendrites. PlexA and Sema2a/2b are known ligands for Sema1a (Sweeney et al., 2011; Yu et al., 2010). However, the

350 dendritic targeting of MBONs was minimally affected in flies homozygous for *sema2a/2b* double
351 mutants or when we knocked down PlexA either pan-neuronally or in glia. Loss of one copy of *plexA*
352 also did not enhance the dendritic targeting defect caused by RNAi knockdown of *sema1a* in
353 MBONs. Therefore, these canonical Sema1a ligands do not seem to play a role in guiding the MBON
354 dendrites. The molecular mechanisms that directing the *sema1a*-positive MBON dendrites to
355 specific MB lobe zones remain unknown.
356

Experimental procedures

Fly strains and husbandry

Fly lines used in this study are (1) *MB077C-splitGAL4* (BDSC:68284)(Aso et al., 2014); (2) *MB091C-splitGAL4* (gift from Y. Aso)(Aso et al., 2014). *MB027B-splitGAL4* (BDSC:68301) (Aso et al., 2014); (3) *MB058B-splitGAL4* (BDSC:68278)(Aso et al., 2014); (4) *MB296B-splitGAL4* (BDSC:68308)(Aso et al., 2014); (5) *MB399C-splitGAL4* (gift from Y. Aso)(Aso et al., 2014); (6) *R53F03-GAL4* (BDSC:48197)(Jenett et al., 2012); (7) *R21D02-GAL4* (BDSC:48939)(Jenett et al., 2012); (8) *R24H08-GAL4* (BDSC:49100)(Jenett et al., 2012); (9) *R25D01-GAL4* (BDSC:49122)(Jenett et al., 2012); (10) *repo-GAL4* (gift from Y-H. Sun); (11) *VT41043-GAL4* (gift from C-L. Wu); (12) *UAS-DenMark,UAS-Dsyd-1::GFP* (Owald et al., 2015); (13) *UAS-mCD8::GFP*(LL4) (Lee and Luo, 1999); (14) *UAS-mCD8::GFP*(II) (Lee and Luo, 1999); (15) *UAS-mCD8::GFP*(III) (Lee and Luo, 1999); (16) *UAS-(FRT stop)myr-SmGdp-HA, UAS-(FRT stop)myr-SmGdp-V5, UAS-(FRT stop)myr-SmGdp-FLAG* (BDSC:64085)(Nern et al., 2015); (17) *MB247-LexA::p65, LexAop-rCD2::RFP* (Awasaki et al., 2011); *LexAop-rCD2::RFP* (II) (Awasaki et al., 2011); (18) *UAS-hid, UAS-rpr* (gift from S. Waddell); (19) UAS-Dicer (VDRC:36148); (20) *20XUAS-FLPG5* (BDSC:55807)(Nern et al., 2011); (21) *R53F03-LexA::p65* (BDSC:53502)(Pfeiffer et al., 2010); (22) *R20G03-LexA::p65* (BDSC:52570)(Pfeiffer et al., 2010); (23) *R25D01-LexA::p65* (BDSC:53519)(Pfeiffer et al., 2010); (24) *12C11-LexA::p65* (BDSC:52444)(Pfeiffer et al., 2010); (25) *hs-FLPG5* (BDSC:77140)(Nern et al., 2011); (26) *UAS-sema1a* (BDSC:65734)(Jeong et al., 2012); (27) *UAS-sema1.mEC-5xmyc* (BDSC:65739)(Jeong et al., 2012); (28) *UAS-sema1.mEC.Fc-5xmyc* (BDSC:65740)(Jeong et al., 2012); (29) *UAS-sema1a-RNAi-1* (BDSC:34320)(Perkins et al., 2015); (30) *UAS-sema1a-RNAi-2* (VDRC:36148)(Dietzl et al., 2007); (31) *UAS-plexA-RNAi* (BDSC:30483)(Pecot et al., 2013; Perkins et al., 2015); (32) *w,ala* (BDSC:9463)(Pascual and Préat, 2001); (33) *plexA*^{EY16548} (BDSC:23097)(Bellen et al., 2011; Shin and DiAntonio, 2011); (34) *40A, sema1a*^{k13702} (Kyoto stock center:111328)(Yu et al., 1998); (35) *Sema2b*^{f02042}*, sema2a*^{p2}*, UAS-mCD8::GFP/CyO* (gift from L. Luo)(Sweeney et al., 2011); (36) *hs-FLP122, 40A, tubp-GAL80* (gift from H-H. Yu); (37) *w; sema1a Artificial exon/CyO; LexAop-tdTomato* (gift from L. Zipursky)(Pecot et al., 2013). The genotypes of the flies used in each figure can be found in Table S1. All flies were reared at 23°C with 60% relative humidity, under a 12 h light: 12 h dark cycle. All our data were derived from male flies.

MARCM and Flip-out

Flies with proper genotypes were heat shocked at 37°C at different developmental stages for different durations (see Table 1S for each of these parameters used in each figure). We waited for at least 3 days after heat-shock to ensure the proper expression of the marker proteins. We then dissected the brains and performed immunofluorescence staining.

Immunofluorescence staining

Fly brains were dissected in phosphate buffered saline (PBS; Sigma, P4417) and fixed in PBS containing 4% formaldehyde (Sigma, F8775) at room temperature for 20 min. The brains were then washed three times with PBS containing 0.5% Triton X-100 (PBST, Sigma-Aldrich, T8787); each time, the brains were incubated in PBST at room temperature for at least 20 min. After that, the brains were incubated in PBST containing 5% normal goat serum (blocking solution; normal goat serum, Jackson ImmunoResearch, 005-000-121) for 30 min at room temperature. After blocking, the brains were incubated in blocking solution containing primary antibodies overnight at 4°C. The next day, the brains were washed three times, 20 min each, with PBST at room temperature before they were incubated in blocking solution containing secondary antibodies overnight at 4°C. The next day, the brain were washed again three times, 20 min each, with PBST at room temperature. Then the brains

were mounted with Gold Antifade reagent (Thermo Fisher Scientific, S36937). Antibodies used in each figure are listed in Table S1. In some cases, we performed sequential staining in which the brains were stained with the first set of primary and secondary antibodies before being incubated with the second set of primary and secondary antibodies. The staining procedures (one time vs. sequential) for each figure are also listed in Table S1. The primary antibodies used in this study are Rat anti-mCD8 (1:100; Invitrogen, MCD0800), Chicken anti-GFP (1:1000; Invitrogen, A10262), Rabbit anti-Dsred (1:100; Takara, 632496), Mouse anti-Trio (1:100; Developmental Studies Hybridoma Bank, DSHB, 9.4A), Mouse anti-FasII (1:100; DSHB, 1D4), Mouse anti-DLG (1:100; DSHB, 4F3), Mouse anti-TH (1:1000; Immunostar, 22941), Rat anti-FLAG (1:200; Novus Biologicals, NBP1-06721), Mouse anti-V5 (1:500; Bio-RAD, MCA1360), and Rabbit anti-V5 (1:500; Abcam, AB9116). The secondary antibodies used in this study are Goat anti-rat-488 (1:400; Jackson ImmunoResearch, 112-545-167), Goat anti-rabbit-Cy3 (1:400; Jackson ImmunoResearch, 111-165-144), Donkey anti-chicken-488 (1:400; Jackson ImmunoResearch, 703-545-155), Goat anti-mouse-Cy5 (1:400; Jackson ImmunoResearch, 115-175-166), Goat anti-mouse-Cy3 (1:400; Jackson ImmunoResearch, 115-165-166), Goat anti-mouse-488 (1:400; Invitrogen, A11029) and Goat anti-rabbit-Cy5 (1:400; Jackson ImmunoResearch, 111-175-144). The stained brains were imaged using a confocal microscope (Zeiss LSM880) and analyzed using Fiji/ImageJ(Schindelin et al., 2012) or Imaris x64 (v9.2.1, Oxford Instruments).

Statistics

Statistical analysis was performed in Prism 8. All data were tested for normality using the Shapiro-Wilk normality test. No data points were excluded from the analysis. Because all our data are normally distributed, we used two-tailed unpaired Student's *t*-test with Welch's correction.

Author contributions

C-H.L. and S.L. conceived the project and designed the experiments. C-H.L. performed the experiments and analyzed the data. S.L. wrote the paper and directed the research.

Acknowledgments

We thank Y. Aso (Janelia Farm Research Campus, USA), G. Rubin (Janelia Farm Research Campus, USA), T. Lee (Janelia Farm Research Campus, USA), L. Luo (Stanford University, USA), Y-H. Sun (Academia Sinica, Taiwan), S. Waddell (University of Oxford, UK), H-H. Yu (Academia Sinica, Taiwan), C-L. Wu (Chang Gung University, Taiwan), L. Zipurski (University of California, Los Angeles, USA), and FlyLight (Janelia Farm Research Campus, USA), the Bloomington Drosophila Stock Center, Vienna Drosophila RNAi center, Harvard TRiP RNAi stock center, Kyoto stock center, and Taiwan Fly Core for fly stocks. S. L. is funded by the Ministry of Science and Technology, Taiwan (107-2311-B-001-042-MY3) and Academia Sinica, Taiwan.

450 # References
451
452 Aso, Y., Hattori, D., Yu, Y., Johnston, R.M., Iyer, N.A., Ngo, T.-T.B., Dionne, H., Abbott, L.F., Axel, R.,
453 Tanimoto, H., et al. (2014). The neuronal architecture of the mushroom body provides a logic for
454 associative learning. Elife *3*, e04577.
455 Awasaki, T., and Ito, K. (2004). Engulfing action of glial cells is required for programmed axon pruning
456 during Drosophila metamorphosis. Curr. Biol. *14*, 668–677.
457 Awasaki, T., Huang, Y., O'Connor, M.B., and Lee, T. (2011). Glia instruct developmental neuronal
458 remodeling through TGF-β signaling. Nat. Neurosci. *14*, 821–823.
459 de Belle, J.S., and Heisenberg, M. (1994). Associative odor learning in Drosophila abolished by
460 chemical ablation of mushroom bodies. Science *263*, 692–695.
461 Bellen, H.J., Levis, R.W., He, Y., Carlson, J.W., Evans-Holm, M., Bae, E., Kim, J., Metaxakis, A., Savakis,
462 C., Schulze, K.L., et al. (2011). The Drosophila gene disruption project: progress using transposons
463 with distinctive site specificities. Genetics *188*, 731–743.
464 Boulanger, A., Clouet-Redt, C., Farge, M., Flandre, A., Guignard, T., Fernando, C., Juge, F., and Dura,
465 J.-M. (2011). ftz-f1 and Hr39 opposing roles on EcR expression during Drosophila mushroom body
466 neuron remodeling. Nat. Neurosci. *14*, 37–44.
467 Boyle, M., Nighorn, A., and Thomas, J.B. (2006). Drosophila Eph receptor guides specific axon
468 branches of mushroom body neurons. Development *133*, 1845–1854.
469 Cafferty, P., Yu, L., Long, H., and Rao, Y. (2006). Semaphorin-1a functions as a guidance receptor in
470 the Drosophila visual system. J. Neurosci. *26*, 3999–4003.
471 Chédotal, A., and Richards, L.J. (2010). Wiring the brain: the biology of neuronal guidance. Cold
472 Spring Harb. Perspect. Biol. *2*, 1–18.
473 Dickson, B.J., and Zou, Y. (2010). Navigating intermediate targets: the nervous system midline. Cold
474 Spring Harb. Perspect. Biol. *2*, a002055.
475 Dietzl, G., Chen, D., Schnorrer, F., Su, K.-C., Barinova, Y., Fellner, M., Gasser, B., Kinsey, K., Oppel, S.,
476 Scheiblauer, S., et al. (2007). A genome-wide transgenic RNAi library for conditional gene
477 inactivation in Drosophila. Nature *448*, 151–156.
478 Evans, T.A. (2016). Embryonic axon guidance: insights from Drosophila and other insects. Curr. Opin.
479 Insect Sci. *18*, 11–16.
480 Godenschwege, T.A., Hu, H., Shan-Crofts, X., Goodman, C.S., and Murphey, R.K. (2002). Bi-directional
481 signaling by Semaphorin 1a during central synapse formation in Drosophila. Nat. Neurosci. *5*, 1294–
482 1301.
483 Grether, M.E., Abrams, J.M., Agapite, J., White, K., and Steller, H. (1995). The head involution
484 defective gene of Drosophila melanogaster functions in programmed cell death. Genes Dev. *9*,
485 1694–1708.
486 Grueber, W.B., Jan, L.Y., and Jan, Y.N. (2002). Tiling of the Drosophila epidermis by multidendritic
487 sensory neurons. Development *129*, 2867–2878.
488 Heisenberg, M. (2003). Mushroom body memoir: from maps to models. Nat. Rev. Neurosci. *4*, 266–
489 275.
490 Hong, W., and Luo, L. (2014). Genetic control of wiring specificity in the fly olfactory system.
491 Genetics *196*, 17–29.
492 Jenett, A., Rubin, G.M., Ngo, T.-T.B., Shepherd, D., Murphy, C., Dionne, H., Pfeiffer, B.D., Cavallaro,
493 A., Hall, D., Jeter, J., et al. (2012). A GAL4-driver line resource for Drosophila neurobiology. Cell Rep.
494 *2*, 991–1001.
495 Jeong, S., Juhaszova, K., and Kolodkin, A.L. (2012). The Control of semaphorin-1a-mediated reverse
496 signaling by opposing pebble and RhoGAPp190 functions in drosophila. Neuron *76*, 721–734.
497 Joiner, W.J., Crocker, A., White, B.H., and Sehgal, A. (2006). Sleep in Drosophila is regulated by adult
498 mushroom bodies. Nature *441*, 757–760.
499 Kolodkin, A.L., and Tessier-Lavigne, M. (2011). Mechanisms and molecules of neuronal wiring: A
500 primer. Cold Spring Harb. Perspect. Biol. *3*, 1–14.

501 Kolodkin, A.L., Matthes, D.J., and Goodman, C.S. (1993). The semaphorin genes encode a family of
502 transmembrane and secreted growth cone guidance molecules. Cell *75*, 1389–1399.
503 Komiyama, T., Sweeney, L.B., Schuldiner, O., Garcia, K.C., and Luo, L. (2007). Graded expression of
504 semaphorin-1a cell-autonomously directs dendritic targeting of olfactory projection neurons. Cell
505 *128*, 399–410.
506 Krashes, M.J., DasGupta, S., Vreede, A., White, B., Armstrong, J.D., and Waddell, S. (2009). A neural
507 circuit mechanism integrating motivational state with memory expression in Drosophila. Cell *139*,
508 416–427.
509 Lee, T., and Luo, L. (1999). Mosaic analysis with a repressible cell marker for studies of gene function
510 in neuronal morphogenesis. Neuron *22*, 451–461.
511 Lee, T., Lee, A., and Luo, L. (1999). Development of the Drosophila mushroom bodies: sequential
512 generation of three distinct types of neurons from a neuroblast. Development *126*, 4065–4076.
513 Lee, T., Marticke, S., Sung, C., Robinow, S., and Luo, L. (2000). Cell-autonomous requirement of the
514 USP/EcR-B ecdysone receptor for mushroom body neuronal remodeling in Drosophila. Neuron *28*,
515 807–818.
516 Lin, S., Huang, Y., and Lee, T. (2009). Nuclear receptor unfulfilled regulates axonal guidance and cell
517 identity of Drosophila mushroom body neurons. PLoS One *4*, e8392.
518 Liu, L.-Y., Long, X., Yang, C.-P., Miyares, R.L., Sugino, K., Singer, R.H., and Lee, T. (2019). Mamo
519 decodes hierarchical temporal gradients into terminal neuronal fate. Elife *8*, 1–28.
520 Liu, Z., Yang, C.-P., Sugino, K., Fu, C.-C., Liu, L.-Y., Yao, X., Lee, L.P., and Lee, T. (2015). Opposing
521 intrinsic temporal gradients guide neural stem cell production of varied neuronal fates. Science *350*,
522 317–320.
523 Marchetti, G., and Tavosanis, G. (2017). Steroid Hormone Ecdysone Signaling Specifies Mushroom
524 Body Neuron Sequential Fate via Chinmo. Curr. Biol. *27*, 3017-3024.e4.
525 Masek, P., and Scott, K. (2010). Limited taste discrimination in Drosophila. Proc. Natl. Acad. Sci. U. S.
526 A. *107*, 14833–14838.
527 Masek, P., Worden, K., Aso, Y., Rubin, G.M., and Keene, A.C. (2015). A dopamine-modulated neural
528 circuit regulating aversive taste memory in Drosophila. Curr. Biol. *25*, 1535–1541.
529 Neckameyer, W.S., and Quinn, W.G. (1989). Isolation and characterization of the gene for Drosophila
530 tyrosine hydroxylase. Neuron *2*, 1167–1175.
531 Nern, A., Pfeiffer, B.D., Svoboda, K., and Rubin, G.M. (2011). Multiple new site-specific recombinases
532 for use in manipulating animal genomes. Proc. Natl. Acad. Sci. *108*, 14198–14203.
533 Nern, A., Pfeiffer, B.D., and Rubin, G.M. (2015). Optimized tools for multicolor stochastic labeling
534 reveal diverse stereotyped cell arrangements in the fly visual system. Proc. Natl. Acad. Sci. U. S. A.
535 *112*, E2967–E2976.
536 Ng, J., Nardine, T., Harms, M., Tzu, J., Goldstein, A., Sun, Y., Dietzl, G., Dickson, B.J., and Luo, L.
537 (2002). Rac GTPases control axon growth, guidance and branching. Nature *416*, 442–447.
538 Owald, D., Felsenberg, J., Talbot, C.B., Das, G., Perisse, E., Huetteroth, W., and Waddell, S. (2015).
539 Activity of defined mushroom body output neurons underlies learned olfactory behavior in
540 Drosophila. Neuron *86*, 417–427.
541 Pascual, A., and Préat, T. (2001). Localization of long-term memory within the Drosophila mushroom
542 body. Science *294*, 1115–1117.
543 Pascual, A., Chaminade, M., and Préat, T. (2005). Ethanolamine kinase controls neuroblast divisions
544 in Drosophila mushroom bodies. Dev. Biol. *280*, 177–186.
545 Pecot, M.Y., Tadros, W., Nern, A., Bader, M., Chen, Y., and Zipursky, S.L. (2013). Multiple interactions
546 control synaptic layer specificity in the Drosophila visual system. Neuron *77*, 299–310.
547 Perkins, L.A., Holderbaum, L., Tao, R., Hu, Y., Sopko, R., McCall, K., Yang-Zhou, D., Flockhart, I., Binari,
548 R., Shim, H.-S., et al. (2015). The Transgenic RNAi Project at Harvard Medical School: Resources and
549 Validation. Genetics *201*, 843–852.
550 Pfeiffer, B.D., Ngo, T.T.B., Hibbard, K.L., Murphy, C., Jenett, A., Truman, J.W., and Rubin, G.M. (2010).
551 Refinement of tools for targeted gene expression in Drosophila. Genetics *186*, 735–755.

552 Pitman, J.L., McGill, J.J., Keegan, K.P., and Allada, R. (2006). A dynamic role for the mushroom bodies
553 in promoting sleep in Drosophila. Nature *441*, 753–756.
554 Plazaola-Sasieta, H., Fernández-Pineda, A., Zhu, Q., and Morey, M. (2017). Untangling the wiring of
555 the Drosophila visual system: developmental principles and molecular strategies. J. Neurogenet. *31*,
556 231–249.
557 Rabinovich, D., Yaniv, S.P., Alyagor, I., and Schuldiner, O. (2016). Nitric Oxide as a Switching
558 Mechanism between Axon Degeneration and Regrowth during Developmental Remodeling. Cell *164*,
559 170–182.
560 Sanes, J.R., and Yamagata, M. (2009). Many paths to synaptic specificity. Annu. Rev. Cell Dev. Biol.
561 *25*, 161–195.
562 Schindelin, J., Arganda-Carreras, I., Frise, E., Kaynig, V., Longair, M., Pietzsch, T., Preibisch, S.,
563 Rueden, C., Saalfeld, S., Schmid, B., et al. (2012). Fiji: an open-source platform for biological-image
564 analysis. Nat. Methods *9*, 676–682.
565 Senapati, B., Tsao, C.-H., Juan, Y.-A., Chiu, T.-H., Wu, C.-L., Waddell, S., and Lin, S. (2019). A neural
566 mechanism for deprivation state-specific expression of relevant memories in Drosophila. Nat.
567 Neurosci. *in press*.
568 Shimizu, K., Sato, M., and Tabata, T. (2011). The Wnt5/planar cell polarity pathway regulates axonal
569 development of the Drosophila mushroom body neuron. J. Neurosci. *31*, 4944–4954.
570 Shin, J.E., and DiAntonio, A. (2011). Highwire regulates guidance of sister axons in the Drosophila
571 mushroom body. J. Neurosci. *31*, 17689–17700.
572 Smith-Trunova, S., Prithviraj, R., Spurrier, J., Kuzina, I., Gu, Q., and Giniger, E. (2015). Cdk5 regulates
573 developmental remodeling of mushroom body neurons in Drosophila. Dev. Dyn. *244*, 1550–1563.
574 SPERRY, R.W. (1963). Chemoaffinity in the orderly growth of nerve fiber patterns and connections.
575 Proc. Natl. Acad. Sci. U. S. A. *50*, 703–710.
576 Sweeney, L.B., Chou, Y.-H., Wu, Z., Joo, W., Komiyama, T., Potter, C.J., Kolodkin, A.L., Garcia, K.C.,
577 and Luo, L. (2011). Secreted semaphorins from degenerating larval ORN axons direct adult
578 projection neuron dendrite targeting. Neuron *72*, 734–747.
579 Takemura, S.-Y., Aso, Y., Hige, T., Wong, A., Lu, Z., Xu, C.S., Rivlin, P.K., Hess, H., Zhao, T., Parag, T., et
580 al. (2017). A connectome of a learning and memory center in the adult Drosophila brain. Elife *6*, 1–
581 43.
582 Tessier-Lavigne, M., and Goodman, C.S. (1996). The molecular biology of axon guidance. Science
583 *274*, 1123–1133.
584 Tsao, C.-H., Chen, C.-C., Lin, C.-H., Yang, H.-Y., and Lin, S. (2018). Drosophila mushroom bodies
585 integrate hunger and satiety signals to control innate food-seeking behavior. Elife *7*, e35264.
586 Vogt, K., Schnaitmann, C., Dylla, K. V, Knapek, S., Aso, Y., Rubin, G.M., and Tanimoto, H. (2014).
587 Shared mushroom body circuits underlie visual and olfactory memories in Drosophila. Elife *3*,
588 e02395.
589 Vogt, K., Aso, Y., Hige, T., Knapek, S., Ichinose, T., Friedrich, A.B., Turner, G.C., Rubin, G.M., and
590 Tanimoto, H. (2016). Direct neural pathways convey distinct visual information to Drosophila
591 mushroom bodies. Elife *5*, e14009.
592 Wang, J., Zugates, C.T., Liang, I.H., Lee, C.-H.J., and Lee, T. (2002). Drosophila Dscam is required for
593 divergent segregation of sister branches and suppresses ectopic bifurcation of axons. Neuron *33*,
594 559–571.
595 White, K., Grether, M.E., Abrams, J.M., Young, L., Farrell, K., and Steller, H. (1994). Genetic control of
596 programmed cell death in Drosophila. Science *264*, 677–683.
597 Winberg, M.L., Noordermeer, J.N., Tamagnone, L., Comoglio, P.M., Spriggs, M.K., Tessier-Lavigne,
598 M., and Goodman, C.S. (1998). Plexin A is a neuronal semaphorin receptor that controls axon
599 guidance. Cell *95*, 903–916.
600 Yu, H.H., Araj, H.H., Ralls, S.A., and Kolodkin, A.L. (1998). The transmembrane Semaphorin Sema I is
601 required in Drosophila for embryonic motor and CNS axon guidance. Neuron *20*, 207–220.
602 Yu, L., Zhou, Y., Cheng, S., and Rao, Y. (2010). Plexin a-semaphorin-1a reverse signaling regulates

603 photoreceptor axon guidance in Drosophila. J. Neurosci. *30*, 12151–12156.
604 Yu, X.M., Gutman, I., Mosca, T.J., Iram, T., Ozkan, E., Garcia, K.C., Luo, L., and Schuldiner, O. (2013).
605 Plum, an immunoglobulin superfamily protein, regulates axon pruning by facilitating TGF-β signaling.
606 Neuron *78*, 456–468.
607 Zhu, S., Lin, S., Kao, C.-F., Awasaki, T., Chiang, A.-S., and Lee, T. (2006). Gradients of the Drosophila
608 Chinmo BTB-zinc finger protein govern neuronal temporal identity. Cell *127*, 409–422.
609 Zwarts, L., Goossens, T., Clements, J., Kang, Y.Y., and Callaerts, P. (2016). Axon Branch-Specific
610 Semaphorin-1a Signaling in Drosophila Mushroom Body Development. Front. Cell. Neurosci. *10*, 210.
611
612

613 # Figure legends

614

615 **Figure 1. Timing of innervations for DANs and MBONs targeting the α'2 zone. (A-F')** The
616 axonal innervation in the MB vertical lobes for PPL1-α'2α2 DANs, labeled by *MB058B-*
617 *splitGAL4* (green), at different hours after puparium formation (APF). The brains were
618 counterstained with *LexAop-rCD2::RFP* driven by *MB247-LexA* (magenta, A'-F'). The white
619 arrowheads in (A-B') indicate where the axons start to innervate the MB lobes. **(G-L')** The
620 dendritic innervation in the MB vertical lobes for MBON-α'2, labeled by *MB091C-splitGAL4*
621 (green), at different hours APF. The brains were counterstained with *LexAop-rCD2::RFP*
622 driven by *MB247-LexA* (magenta, G'-L'). The white arrowheads in (K-K') indicate where the
623 dendrites start to innervate the MB lobes. **(M-M'')** 3-D images of the PPL1-α'2α2 axons in
624 the MB lobes. Axons were labeled with *UAS-mCD8::GFP* driven by *MB058B-splitGAL4* (green,
625 M-M'') and all MB lobe were labeled with *LexAop-rCD2::RFP* driven by *MB247-LexA*
626 (magenta, M'-M'') and the α and β lobes were labeled with anti-FasII antibody (blue, M-
627 M''). The white arrowheads in (M-M') indicate the axonal processes extending at the
628 junctions between α and α' lobes. Scale bar in (A-L'): 50 µm. Scale bar in (M-M''): 15 µm.
629 Detailed genotypes are listed in Table S1.

630

631 **Figure 2. Ablation of PPL1-α'2α2 DANs has no effect on the MB-targeting of neighboring**
632 **DANs and MBON-α'2. (A-A''')** A wild-type brain whose PPL1-α'2α2 DANs were labeled with
633 *UAS-mCD8::GFP* driven by *MB058B-splitGAL4* (green, A and A''') and MBON-α'2, with
634 *LexAop-rCD2::RFP* driven by *R20G03-LexA* (magenta, A'' and A'''). The brain was also
635 counterstained with anti-TH antibody (blue, A' and A'''). A single focal plane is shown. The
636 white dashed circle in (A') and the white arrowhead in (A''') indicate the α'2 zone. **(B-B''')**
637 Same as (A-A''') except that PPL1-α'2α2 DANs were ablated with *UAS-rpr,hid* driven by
638 *MB058B-splitGAL4*. **(C-C'')** A wild-type brain whose MBON-α'2 was labeled with *UAS-*
639 *mCD8::GFP* driven by *MB091C-splitGAL4* (green, C and C'') and MBON-α'3, with *LexAop-*
640 *rCD2::RFP* driven by *R53F03-LexA* (magenta, C' and C''). The brain was also counterstained
641 with anti-Trio antibody labeling α', β' and γ lobes (blue, C''). The white arrowhead in (C'')
642 indicates the α'3 zone. **(D-D'')** Same as (C-C'') except that MBON-α'2 was ablated with *UAS-*
643 *rpr,hid* driven by *MB091C-splitGAL4*. **(E-E'')** A wild-type brain whose MBON-α'2 was labeled
644 with *UAS-mCD8::GFP* driven by *MB091C-splitGAL4* (green, E and E'') and MBON-γ2α'1, with
645 *LexAop-rCD2::RFP* driven by *R25D01-LexA* (magenta, E' and E''). The brain was also
646 counterstained with anti-Trio antibody labeling α', β' and γ lobes (blue, E''). A single focal
647 plane is shown. The white arrowhead in (E'') indicates the α'1 zone. **(F-F'')** Same as (E-E'')
648 except that MBON-α'2 was ablated with *UAS-rpr,hid* driven by *MB091C-splitGAL4*. Scale
649 bars: 50 µm. Detailed genotypes are listed in Table S1.

650

651 **Figure 3. Ablation of MBON-α'3 impairs the development of the α' lobe. (A-A''')** A wild-
652 type brain whose MBON-α'3 was labeled with *UAS-mCD8::GFP* driven by *MB027B-splitGAL4*
653 (green, A and A''') and all KCs, with *LexAop-rCD2::RFP* driven by *MB247-LexA* (magenta, A''
654 and A'''). The brain was also counterstained with anti-Trio antibody labeling α', β' and γ
655 lobes (blue, A'). The white arrowheads in (A'-A''') indicate the α'3 zone. **(B-B''')** Same as (A-
656 A''') except that MBON-α'3 was ablated with *UAS-rpr,hid* driven by *MB027B-splitGAL4*. **(C)**
657 The parameters used to measure the position of the α'3 zone relative to the α lobe tip (*h*
658 and *d*) and the width of the α'2 zone (*w*). *d* was measured by the horizontal distance

659 between the most lateral position of the α′3 zone and the middle of the α lobe tip. *h* was
660 measured by the vertical distance between the α and α′ lobe tips. *w* was measured as the
661 horizontal distance between two points, one on the inner border and the other on the outer
662 border of the α′2 zone. The points were selected as the position closest to the brain midline
663 on each border. **(D)** The lateral position of the α′3 zone (*d*) was reduced when MBON-α′3
664 was ablated (p<0.0001, n = 10, two-tailed unpaired *t*-test with Welch's correction). **(E)** The
665 relative height of the α′ lobe (*h*) was reduced when MBON-α′3 was ablated (p=0.0009, n =
666 10, two-tailed unpaired *t*-test with Welch's correction). **(F)** The growth of the α′ lobe was
667 impaired when MBON-α′3 was ablated. The growth was measured by the relative positions
668 of the tips of α and α′ lobes (*h*) at 24, 48, and 72 h APF. (24 h APF: p=0.7224, n = 6; 48 h APF:
669 p=0.0263, n = 6; 72 h APF: p=0.002, n = 6; two-tailed unpaired *t*-test with Welch's
670 correction). **(G-G'')** A wild-type brain whose MBON-α′3 was labeled with *UAS-mCD8::GFP*
671 driven by *MB027B-splitGAL4* (green, G and G'') and MBON-α′2, with *LexAop-rCD2::RFP*
672 driven by *R20G03-LexA* (magenta, G' and G''). The brain was also counterstained with anti-
673 Trio antibody labeling α′, β′ and γ lobes (blue, G''). The white arrowheads in (G'') indicate
674 the α′2 zone. **(H-H'')** Same as (G-G'') except that MBON-α′3 was ablated with *UAS-rpr,hid*
675 driven by *MB027B-splitGAL4*. **(I)** The width of the α′2 zone (*w*) was not changed when
676 MBON-α′2 was ablated (p=0.3051, n = 10, two-tailed unpaired *t*-test with Welch's
677 correction). Scale bars: 50 µm. Detailed genotypes are listed in Table S1.
678
679 **Figure 4. Loss of vertical lobes results in mistargeted PPL1-α′2α2 axons. (A-B'')** Single-cell
680 flip-out clones of PPL1-α′2α2 DANs (green; A, A'', B, and B'') in *ala* mutant brain where the
681 MB lost its vertical lobes on the ipsilateral (A-A'') or contralateral (B-B'') side to the clones.
682 The brains were counterstained with anti-Trio and anti-FasII antibodies to label all MB lobes
683 (magenta; A'-A'' and B'-B''). The white arrowheads in (A, A'', B and B'') indicate the
684 mistargeted axons. **(C-C')** The axonal innervation patterns of PPL1-α′2α2 DANs in an *ala*
685 mutant brain at 30 h APF. The PPL1-α′2α2 DANs were labeled with *UAS-mCD8::GFP* driven
686 by *MB058B-splitGAL4* (green), and all KCs were labeled with *LexAop-rCD2::RFP* driven by
687 *MB247-LexA* (magenta, C'). The vertical lobes were missing in one hemibrain. The white
688 arrowheads indicate the mistargeted neurites near the missing lobes. **(D-D')** A single focal
689 plane from (C-C') showing the α′2/α2 zones. The white arrowheads indicate the mistargeted
690 neurites locate laterally and dorsally to the putative missing α′2/α2 zones. Scale bars: 50
691 µm. Detailed genotypes are listed in Table S1.
692
693 **Figure 5. MBON-α′2 dendrites innervate other MB lobe zones when their normal target**
694 **zone is missing. (A-A'')** Dendritic innervation pattern of MBON-α′2 labeled with *UAS-*
695 *mCD8::GFP* driven by *MB091C-splitGAL4* (green, A and A'') in an *ala* mutant brain where
696 vertical lobes were missing in one hemibrain. The KCs were labeled with *LexAop-rCD2::RFP*
697 driven by *MB247-LexA* (magenta, A' and A''). White arrowheads in (A and A'') indicate α′1
698 and β′2mp zones. **(B-B'')** Same as (A-A''), except that the MBON-α′2 was labeled with *UAS-*
699 *dSyd-1-GFP* (green, presynaptic marker, B and B'') and *UAS-DenMark* (magenta,
700 postsynaptic marker, B' and B''). White arrowheads in (B' and B'') indicate α′1 and β′2mp
701 zones. **(C-E')** The dendritic targeting of MBON-α′2 labeled with *UAS-mCD8::GFP* driven by
702 *MB091C-splitGAL4* (green) in *ala* mutant brains at 36 (C-C'), 48 (D-D'), and 72 (E-E') h APF.
703 The KCs were labeled with *LexAop-rCD2::RFP* driven by *MB247-LexA* (magenta, C', D' and E').
704 Vertical lobes were missing in one hemibrain. The white arrowheads in (D-D') indicate the

705 α′2 zone, and the arrowheads in (E-E′) indicate the ectopic innervations of the MBON-α′2
706 dendrites. Scale bars: 50 µm. Detailed genotypes are listed in Table S1.
707
708 **Figure 6. Overexpression of *sema1a* redirects PPL1-α′2α2 and PPL1-γ2α′1 dendrites to**
709 **distinct MB lobe zones. (A-A′′)** PPL1-α′2α2 DANs labeled with *UAS-mCD8::GFP* driven by
710 *MB058B-splitGAL4* (green, A and A′′) in a wild-type brain. The brain was counterstained with
711 anti-Trio and anti-FasII antibodies to label all MB lobes (magenta, A′ and A′′). **(B-B′′)** Same as
712 (A-A′′) except that Sema1a was additionally overexpressed in PPL1-α′2α2 DANs with *UAS-*
713 *sema1a* driven by *MB058B-splitGAL4*. Arrowheads in (B and B′′) indicate β′2p, α′1, and α′3
714 zones. **(C-C′′)** Same as (B-B′′) but the *UAS-sema1a* was replaced with *UAS-sema1.mEC-5xmyc*.
715 **(D-D′′)** Same as (B-B′′) but the *UAS-sema1a* was replaced with *UAS-sema1.mEC.Fc-5xmyc*. **(E-**
716 **E′′)** Same as (B-B′′), except that the PPL1-α′2α2 DANs were labeled with *UAS-dSyd-1-GFP*
717 (green, presynaptic marker, E and E′′) and *UAS-DenMark* (magenta, postsynaptic marker, E′
718 and E′′). Arrowheads in (E′ and E′′) indicate β′2p, α′1, and α′3 zones. **(F-F′′)** PPL1-γ2α′1 DANs
719 labeled with *UAS-mCD8::GFP* driven by *MB296B-splitGAL4* (green, F and F′′) in a wild-type
720 brain. The brain was counterstained with anti-Trio and anti-FasII antibodies to label all MB
721 lobes (magenta, F′ and F′′). **(G-G′′)** Same as (F-F′′) except that Sema1a was additionally
722 overexpressed in PPL1-γ2α′1 DANs with *UAS-sema1a* driven by *MB296B-splitGAL4*.
723 Arrowheads in (G and G′′) indicates β′2mp and β′2a zones. **(H-H′′)** A single focal plane from
724 (G-G′′) showing the innervation of ectopic PPL1-γ2α′1 neurites in the β′2a zone (outlined by
725 white dashed lines, F and F′′). **(I-I′′)** Same as (G-G′′), except that the PPL1-γ2α′1 DANs were
726 labeled with *UAS-dSyd-1-GFP* (green, I and I′′) and *UAS-DenMark* (magenta, I′ and I′′).
727 Arrowheads in (I′ and I′′) indicate the β′2mp and β′2a zones. Scale bars: 50 µm. Detailed
728 genotypes are listed in Table S1.
729
730 **Figure 7. Mistargeting of MBON-α′2 dendrites resulted from missing vertical lobes**
731 **requires *sema1a*. (A-A′′)** The dendritic innervation pattern of MBON-α′2 labeled with *UAS-*
732 *mCD8::GFP* driven by *MB091C-splitGAL4* (green, A and A′′) in a *ala* mutant brain where MB
733 vertical lobes were lacking in one hemibrain. All MB lobes were labeled with *LexAop-*
734 *rCD2::RFP* driven by *MB247-LexA* (magenta, A′ and A′′). **(B-B′′)** Same as (A-A′′), except that
735 *UAS-sema1a-RNAi* was additionally expressed in MBON-α′2. The white arrowheads in
736 indicate the mistargeted dendrites in the β′2 and α′1 zones and the yellow arrowheads
737 indicate the normal innervation in the α′2 zones. Note that the ectopic dendritic
738 innervations were largely reduced and the normal α′2 innervation is not affected by the
739 knockdown of *sema1a*. Scale bars: 50 µm. Detailed genotypes are listed in Table S1.
740
741 **Figure 8. *sema1a* is required for the dendritic targeting of MBON-β2β′2a, MBON-α′3 and**
742 **MBON-α′1. (A-A′′)** The dendritic innervation pattern of MBON-β2β′2a labeled with *UAS-*
743 *mCD8::GFP* driven by *MB399C-splitGAL4* (green, A-A′′). The α′, β′ and γ lobes were labeled
744 with anti-Trio antibody (magenta, A′ and A′′). The β′2a zones are outlined with white dashed
745 circles, and the β2 zones are indicated by yellow arrowheads. (A′′) is a high magnification
746 view of a single focal plane showing the β′2a and β2 zones. **(B-B′′)** Same as (A-A′′), except
747 that *UAS-sema1a-RNAi-1* was additionally expressed by *MB399C-splitGAL4* in MBON-
748 β2β′2a. The white arrowhead in (B) indicate the mistargeted neurites. **(C-D)** Wild-type (C)
749 and *UAS-sema1a-RNAi-1*-expressed (D) MBON-β2β′2a labeled with dSyd-1-GFP (green,
750 presynaptic marker) and DenMark (magenta, postsynaptic marker) driven by *MB399C-*
751 *splitGAL4*. The brains were counterstained with anti-Trio and anti-FasII antibodies to label all

752 MB lobes (blue). The white arrowhead in (D) indicates the mistargeted dendrites. **(E-F')**
753 Wild-type (E-E') and *UAS-sema1a-RNAi*-1-expressed (F-F') MBON-α'3 labeled with *UAS-*
754 *mCD8::GFP* driven by *MB027B-splitGAL4* (green) The brains were counterstained with anti-
755 Trio antibody to label the α', β' and γ lobes (magenta, E' and F'). The white arrowhead in (F)
756 indicate the mistargeted dendrites. **(G-H)** Wild-type (G) and *UAS-sema1a-RNAi-1*-expressed
757 (H) MBON-α'3 labeled with dSyd-1-GFP (green, presynaptic marker) and DenMark (magenta,
758 postsynaptic marker) driven by *MB027B-splitGAL4*. The brains were counterstained with
759 anti-Trio and anti-FasII antibodies to label all MB lobes (blue). The white arrowhead in (D)
760 indicate the mistargeted dendrites.
761
762 **Figure 9. *sema1a* mutant MARCM clones for MBON-β2β'2a, MBON-α'3 and MBON-α'1**
763 **exhibit defective dendritic targeting. (A-B')** Wild-type (A-A') and *sema1a*^{k13702} (B-B')
764 MARCM clones for MBON-β2β'2a labeled with *UAS-mCD8::GFP* driven by *R21D02-GAL4*
765 (green). The brains were counterstained with anti-Trio antibody to label the α', β' and γ
766 lobes (magenta, A' and B') The white arrowheads in (B-B') indicate the mistargeted
767 dendrites. **(C-D')** Wild-type (C-C') and *sema1a*^{k13702} (D-D') MARCM clones for MBON-α'3
768 labeled with *UAS-mCD8::GFP* driven by *R53F03-GAL4* (green). The brains were
769 counterstained with anti-Trio antibody to label the α', β' and γ lobes (magenta, C' and D').
770 The white arrowhead in (D-D') indicates the mistargeted dendrites. **(E-F')** Wild-type (E-E')
771 and *sema1a*^{k13702} (F-F') MARCM clones for MBON-α'3 and MBON-α'1 labeled with *UAS-*
772 *mCD8::GFP* driven by *R24H08-GAL4* (green). The brains were counterstained with anti-Trio
773 antibody to label the α', β' and γ lobes (magenta, E' and F') The yellow arrowheads in (E-E')
774 indicates the innervation of MBON-α'3 and white arrowhead in the same images indicate
775 the innervation of MBON-α'1. Note the MBON-α'3 was always accompanied by MBON-α'1
776 in the wild-type MARCM clones (n = 17), indicating they are in the same lineage. Both
777 MBON-α'3 and MBON-α'1 innervations were defective in *sema1a*^{k13702} MARCM clones (F-F').
778 **(G-H')** Wild-type (G-G') and *sema1a*^{k13702} (H-H') MARCM clones for MBON-β'2mp labeled
779 with *UAS-mCD8::GFP* driven by *VT41043-GAL4* (green). The brains were counterstained with
780 anti-Trio antibody to label the α', β' and γ lobes (magenta, G' and H'). The white arrowheads
781 in (H-H') indicate the mistargeted dendrites. Scale bars: 50 µm. Detailed genotypes are
782 listed in Table S1.
783
784 **Figure 10. Canonical Sema1a ligands are not required for the dendritic targeting of**
785 **MBONs. (A-A')** MBONs innervating the β'2mp, β'2a and β2 zones (indicated by white
786 arrowheads and a dashed circle) were labeled with *UAS-mCD8::GFP* driven by *R21D02-GAL4*
787 (green) in a *Sema2b*^{f02042}*, sema2a*^{p2} double mutant brain. The brain was counterstained with
788 anti-Trio antibody to label α', β', and γ lobes (magenta, A'). A signal focal plane is shown.
789 Note the dendritic innervations in the MB lobe zones were largely unaffected. **(B-B')** The
790 dendritic innervation of MBON-α'3 labeled with *UAS-mCD8::GFP* driven by *R53F03-GAL4*
791 (green) in a *Sema2b*^{f02042}*, sema2a*^{p2} double mutant brain. The brain was counterstained with
792 anti-Trio antibody to label α', β', and γ lobes (magenta, B'). Note that although the α' lobe
793 tip is enlarged, the MBON-α'3 dendrites are largely confined in the α'3 zone (indicated by
794 white arrowheads). **(C-D')** MBON-α'3 expressing *UAS-sema1a-RNAi-2* and *UAS-mCD8::GFP*
795 driven by *MB027B-splitGAL4* (green) in a wild-type (C-C') or a *plexA*^{EY16548} heterozygous
796 mutant brain (D-D'). The brains were counterstained with anti-Trio and anti-FasII antibodies
797 to label all MB lobes (magenta, C' and D'). White arrowheads indicate the mistargeted
798 dendrites. Note the dendritic mistargeting phenotype was not enhanced in the *plexA*^{EY16548}

heterozygous mutant brain (compare C and D to Fig. 8E). **(E-F')** MBON-β2β'2a expressing *UAS-sema1a-RNAi-2* and *UAS-mCD8::GFP* driven by *MB0399C-splitGAL4* (green) in a wild-type (E-E') or a *plexA*^{EY16548} heterozygous mutant brain (F-F'). The brains were counterstained with anti-Trio and anti-FasII antibodies to label all MB lobes (magenta, E' and F'). White arrowheads indicate the mistargeted dendrites. Note the dendritic mistargeting phenotype was not enhanced in the *plexA*^{EY16548} heterozygous mutant brain (compare E and F to Fig. 8A). **(G-H')** MBONs innervating the β'2mp, β'2a and β2 zones (indicated by white arrowheads and a dashed circle) were labeled with *LexAop-rCD2::RFP* driven by *R12C11-LexA* (magenta) in a wild-type brain (G-G') or a brain where *UAS-plexA-RNAi* was expressed pan-neuronally by *nSyb-GAL4* (H-H'). The brains were counterstained with anti-Trio and anti-FasII antibodies to label all MB lobes (green, G'and H'). **(I-J')** MBON-α'3 was labeled with *LexAop-rCD2::RFP* driven by *R53F03-LexA* (magenta) in a wild-type brain (I-I') or a brain where *UAS-plexA-RNAi* was expressed pan-neuronally by *nSyb-GAL4* (J-J'). The brains were counterstained with anti-Trio and anti-FasII antibodies to label all MB lobes (green, I'and J'). The white arrowheads indicate the α'3 zones. **(K-N')** Same as (G-J'), except that *UAS-plexA-RNAi* was expressed in all glia using *repo-GAL4* (L-L' and N-N'). Scale bars: 50 µm. Detailed genotypes are listed in Table S1.

Figure 1

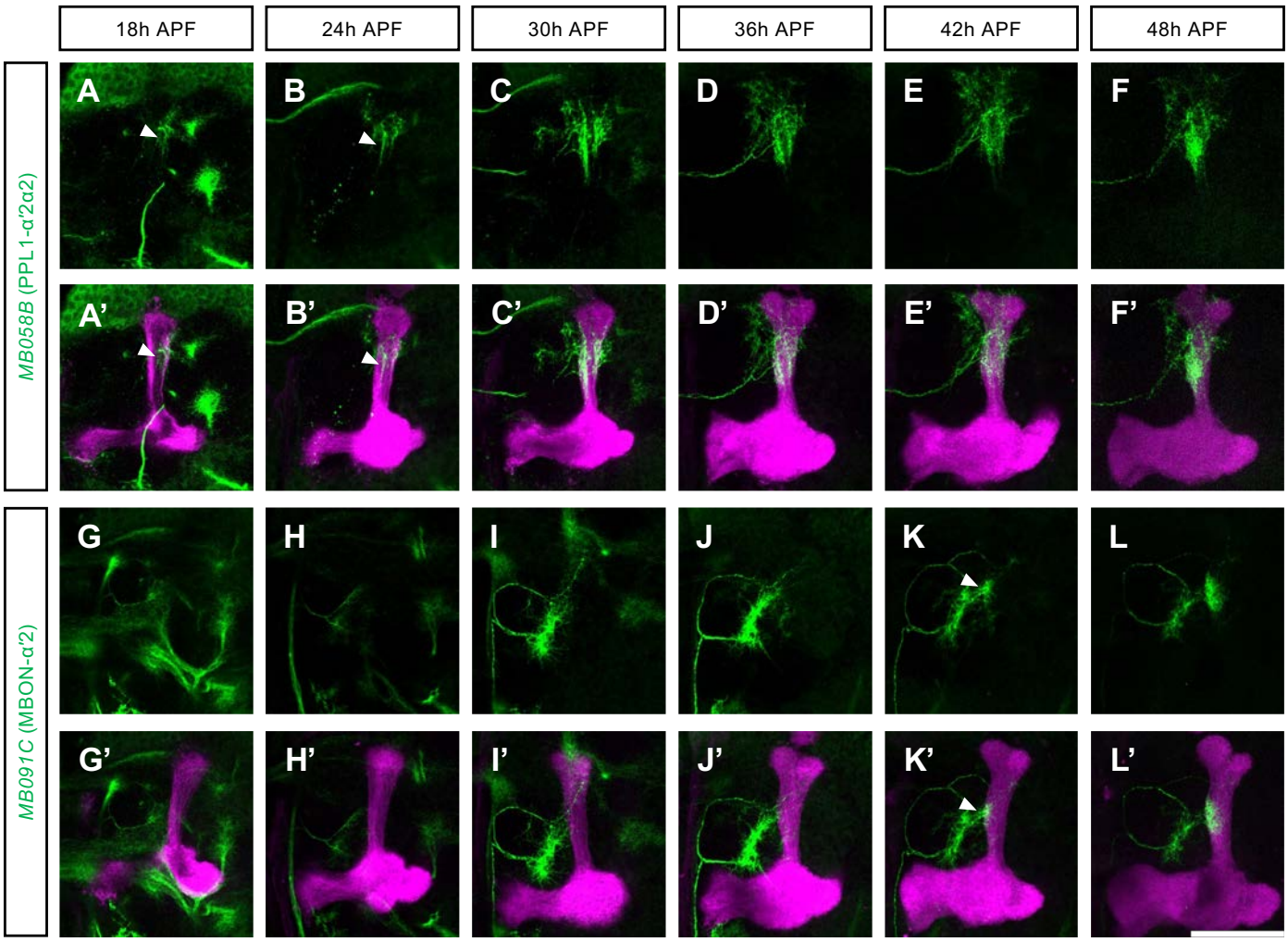
18h APF
24h APF
30h APF
36h APF
42h APF
48h APF
MB058B (PPL1-α′2α2)
MB091C (MBON-α′2)
A
B
C
D
E
F
A’
B’
C’
D’
E’
F’
G
H
I
J
K
L
G’
H’
I’
J’
K’
L’

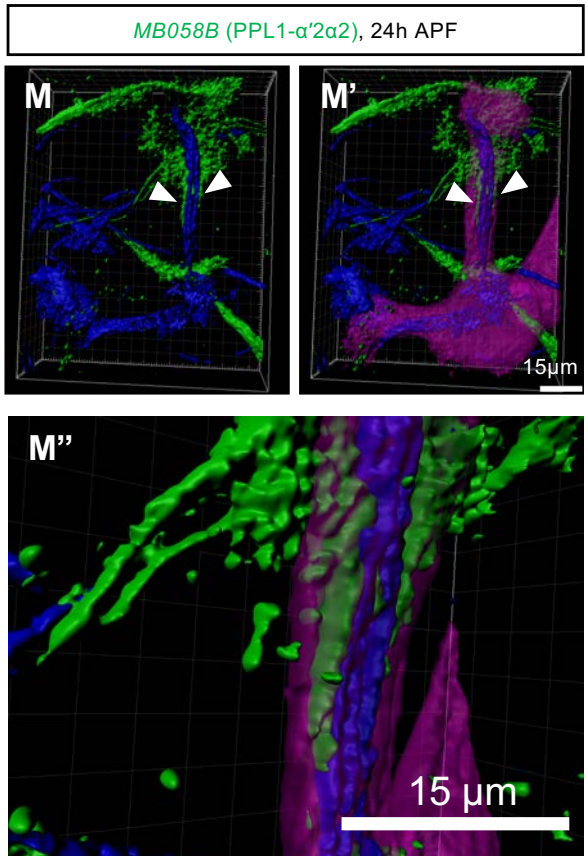
MB058B (PPL1-α′2α2), 24h APF
M
M’
15µm
M”
15 µm

Figure 2

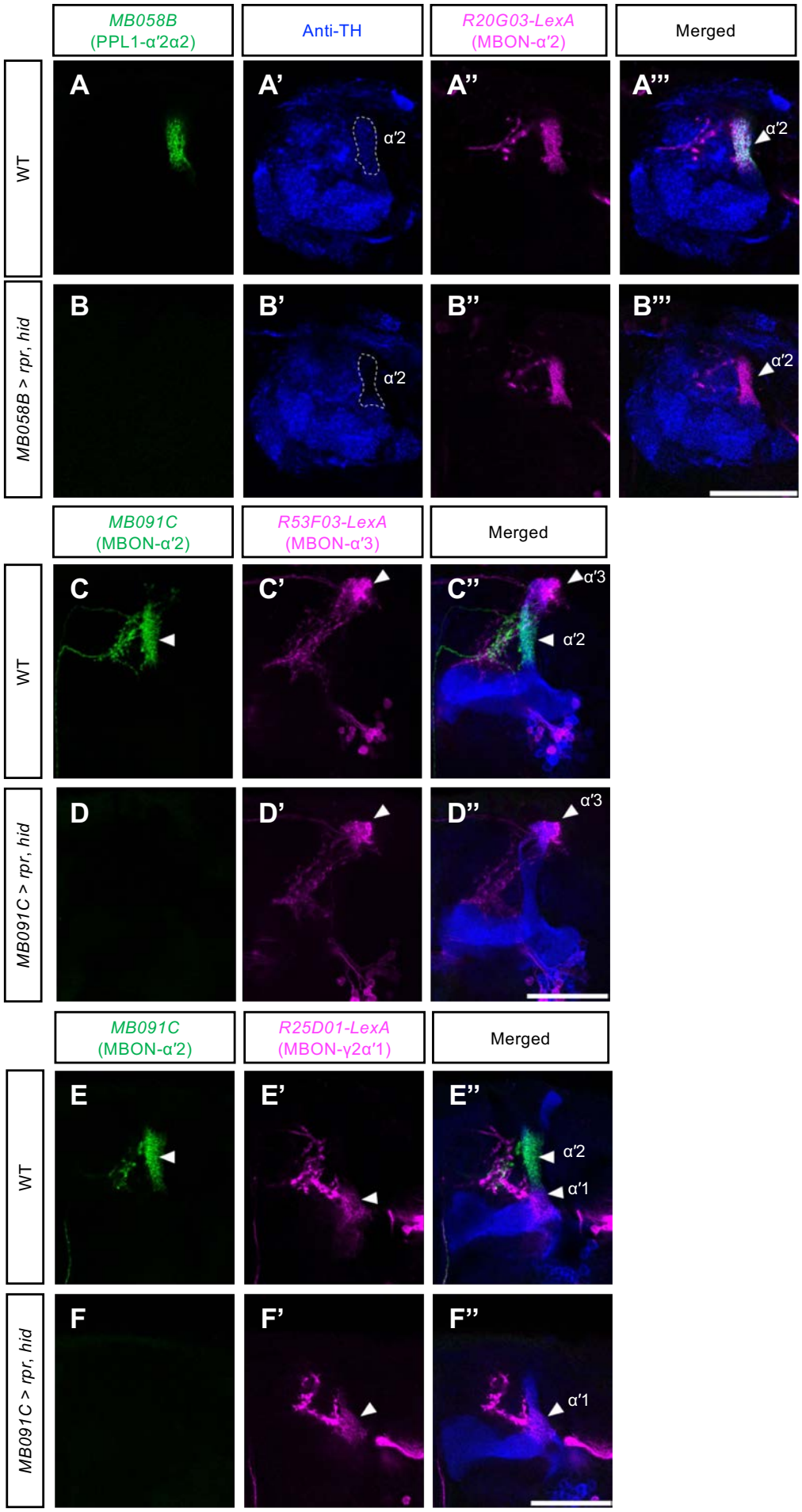
MB058B
(PPL1-α′2α2)
Anti-TH
R20G03-LexA
(MBON-α′2)
Merged
WT
MB058B > rpr, hid
A
A’
A”
A’”
B
B’
B”
B’”
α′2
MB091C
(MBON-α′2)
R53F03-LexA
(MBON-α′3)
C
C’
C”
D
D’
D”
α′3
R25D01-LexA
(MBON-γ2α′1)
E
E’
E”
F
F’
F”
α′1
MB091C > rpr, hid

Figure 3

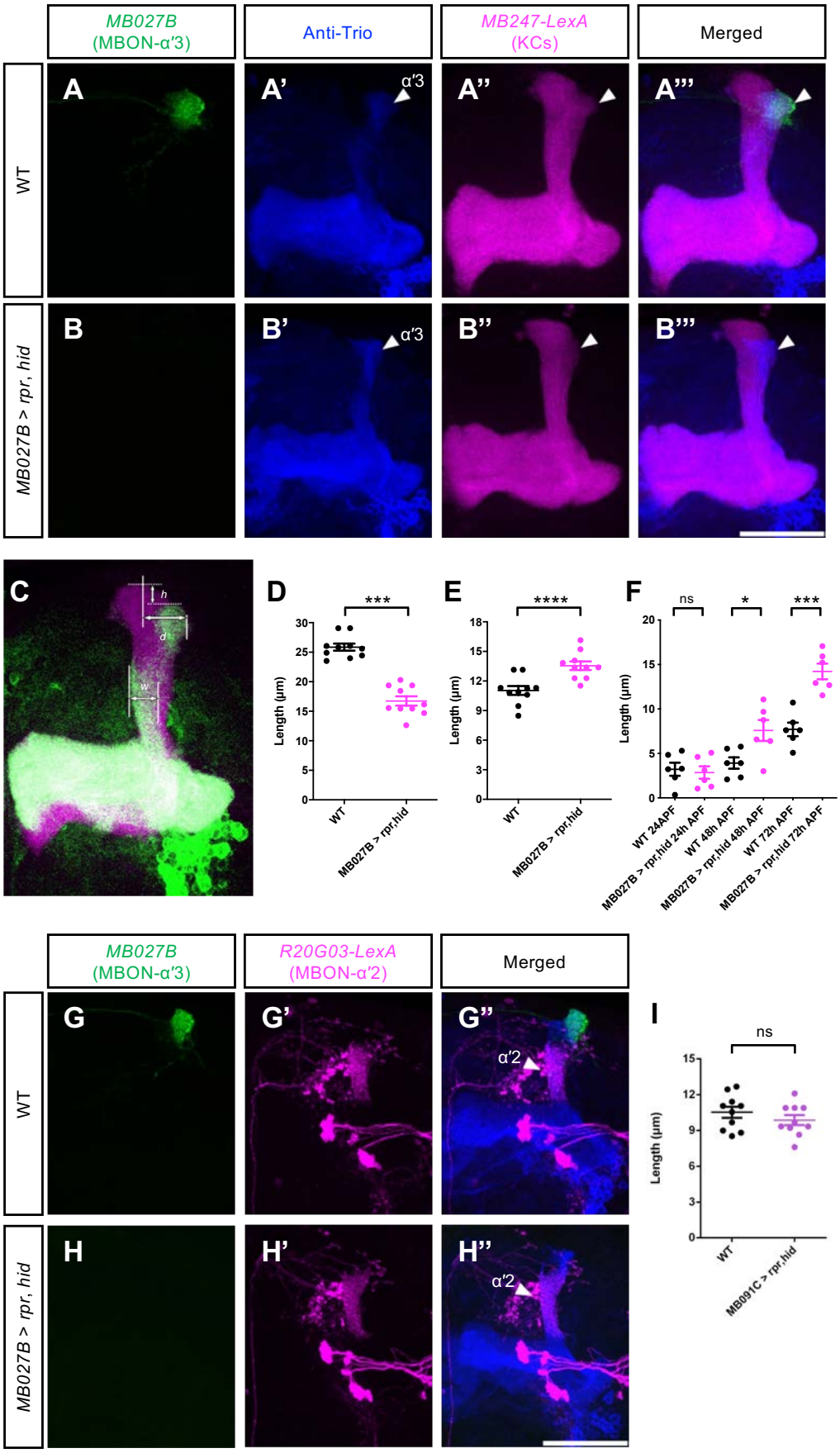
MB027B
(MBON-α′3)
Anti-Trio
MB247-LexA
(KCs)
Merged
WT
MB027B > rpr, hid
A
A'
α′3
A''
A'''
B
B'
α′3
B''
B'''
C
h
d
w
D
***
Length (μm)
WT
MB027B > rpr,hid
E
****
Length (μm)
WT
MB027B > rpr,hid
F
ns
*
***
Length (μm)
WT 24APF
MB027B > rpr,hid 24h APF
WT 48h APF
MB027B > rpr,hid 48h APF
WT 72h APF
MB027B > rpr,hid 72h APF
MB027B
(MBON-α′3)
R20G03-LexA
(MBON-α′2)
Merged
WT
MB027B > rpr, hid
G
G'
G''
α′2
H
H'
H''
α′2
I
ns
Length (μm)
WT
MB091C > rpr,hid

Figure 4

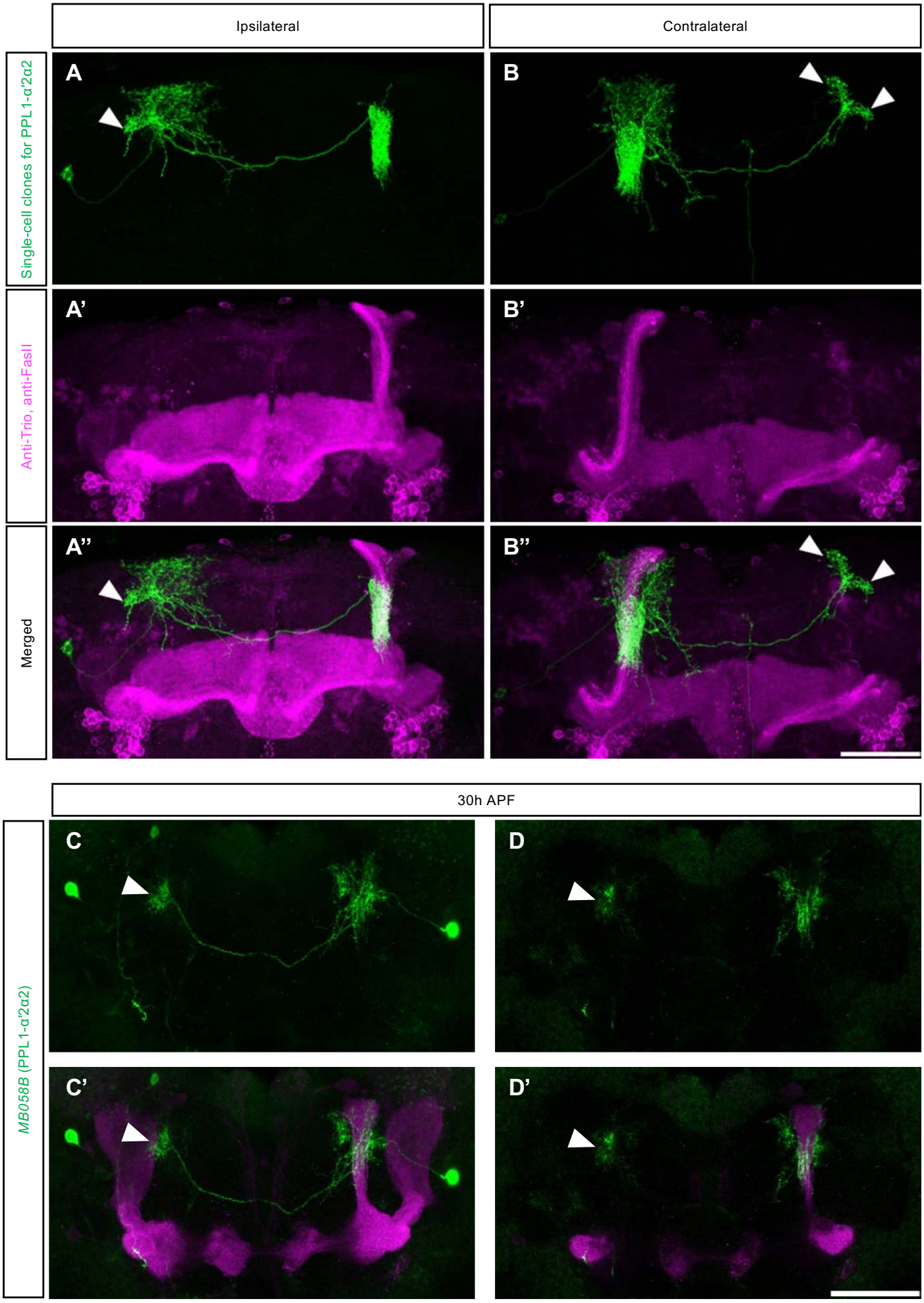
Ipsilateral
Contralateral
Single-cell clones for PPL1-α'2α2
Anti-Trio, anti-FasII
Merged
A
B
A'
B'
A''
B''
30h APF
MB058B (PPL1-α'2α2)
C
D
C'
D'

Figure 5

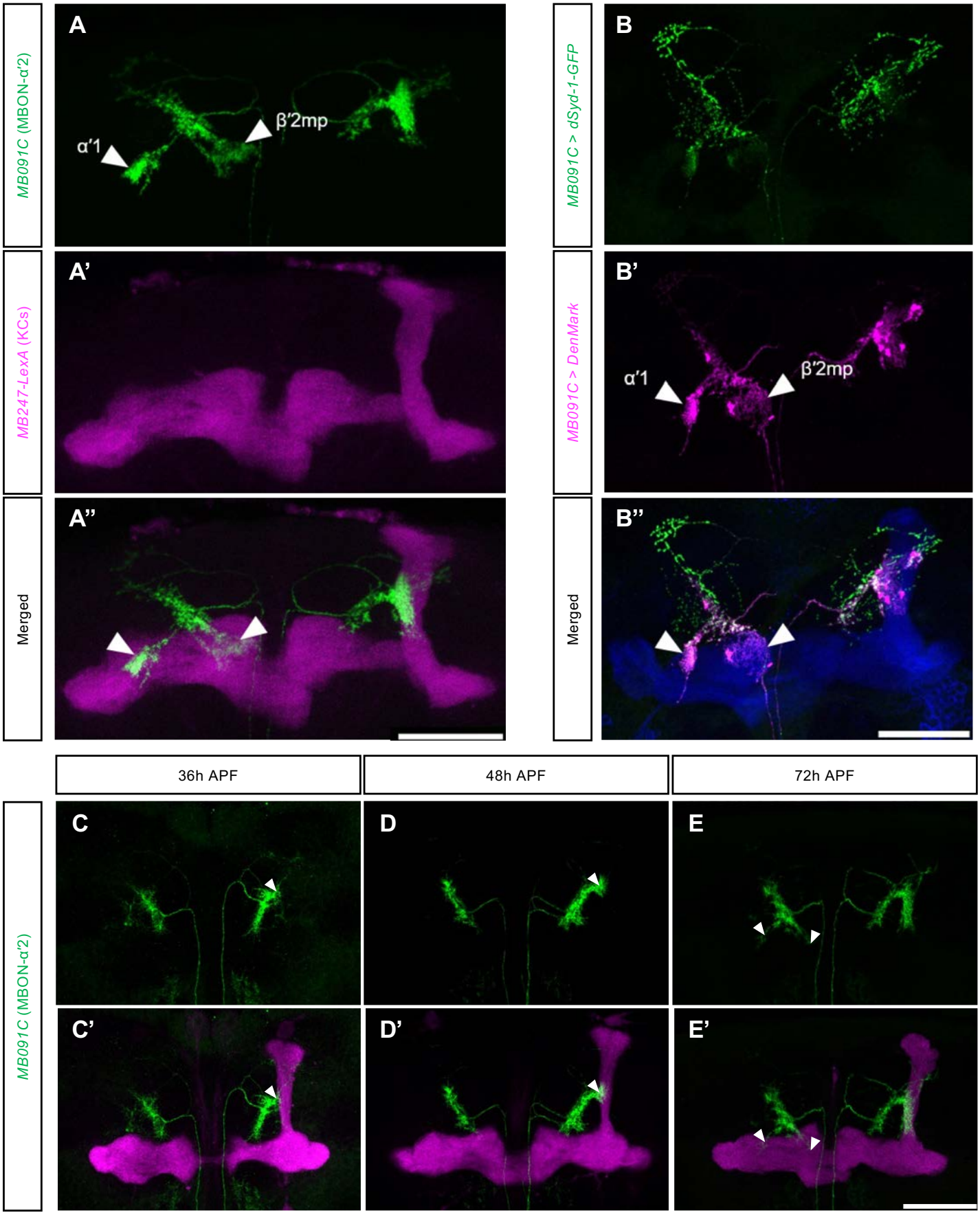
MB091C (MBON-α'2)
A
α'1
β'2mp
MB091C > dSyd-1-GFP
B
MB247-LexA (KCs)
A'
MB091C > DenMark
B'
α'1
β'2mp
Merged
A''
Merged
B''
36h APF
48h APF
72h APF
MB091C (MBON-α'2)
C
D
E
C'
D'
E'

Figure 6

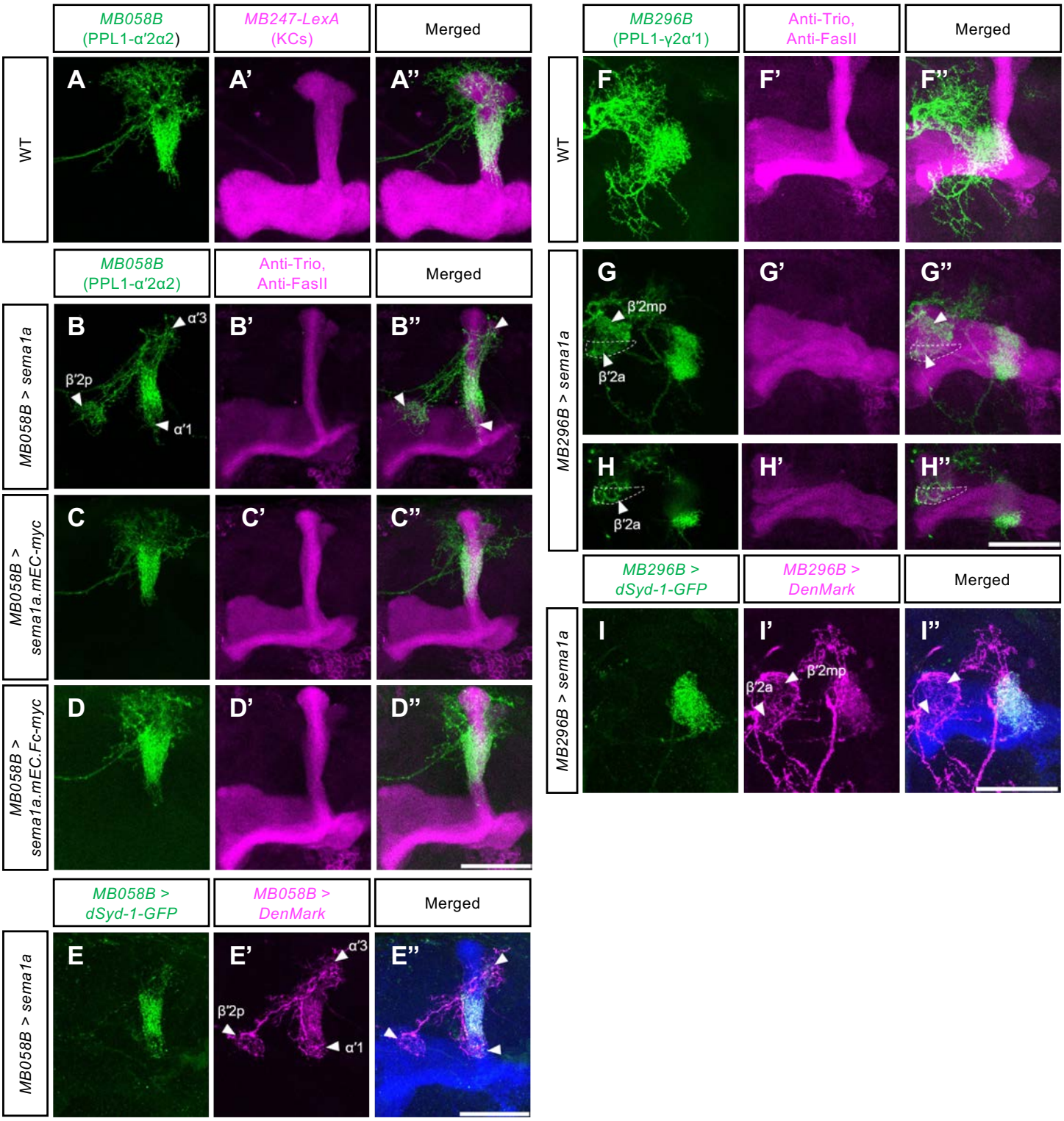
MB058B (PPL1-α′2α2)
MB247-LexA (KCs)
Merged
WT
A
A’
A”
MB058B (PPL1-α′2α2)
Anti-Trio, Anti-FasII
Merged
MB058B > sema1a
B
B’
B”
α′3
β′2p
α′1
MB058B > sema1a.mEC-myc
C
C’
C”
MB058B > sema1a.mEC.Fc-myc
D
D’
D”
MB058B > dSyd-1-GFP
MB058B > DenMark
Merged
MB058B > sema1a
E
E’
E”
α′3
β′2p
α′1
MB296B (PPL1-γ2α′1)
Anti-Trio, Anti-FasII
Merged
WT
F
F’
F”
MB296B > sema1a
G
G’
G”
β′2mp
β′2a
H
H’
H”
β′2a
MB296B > dSyd-1-GFP
MB296B > DenMark
Merged
MB296B > sema1a
I
I’
I”
β′2mp
β′2a

Figure 7

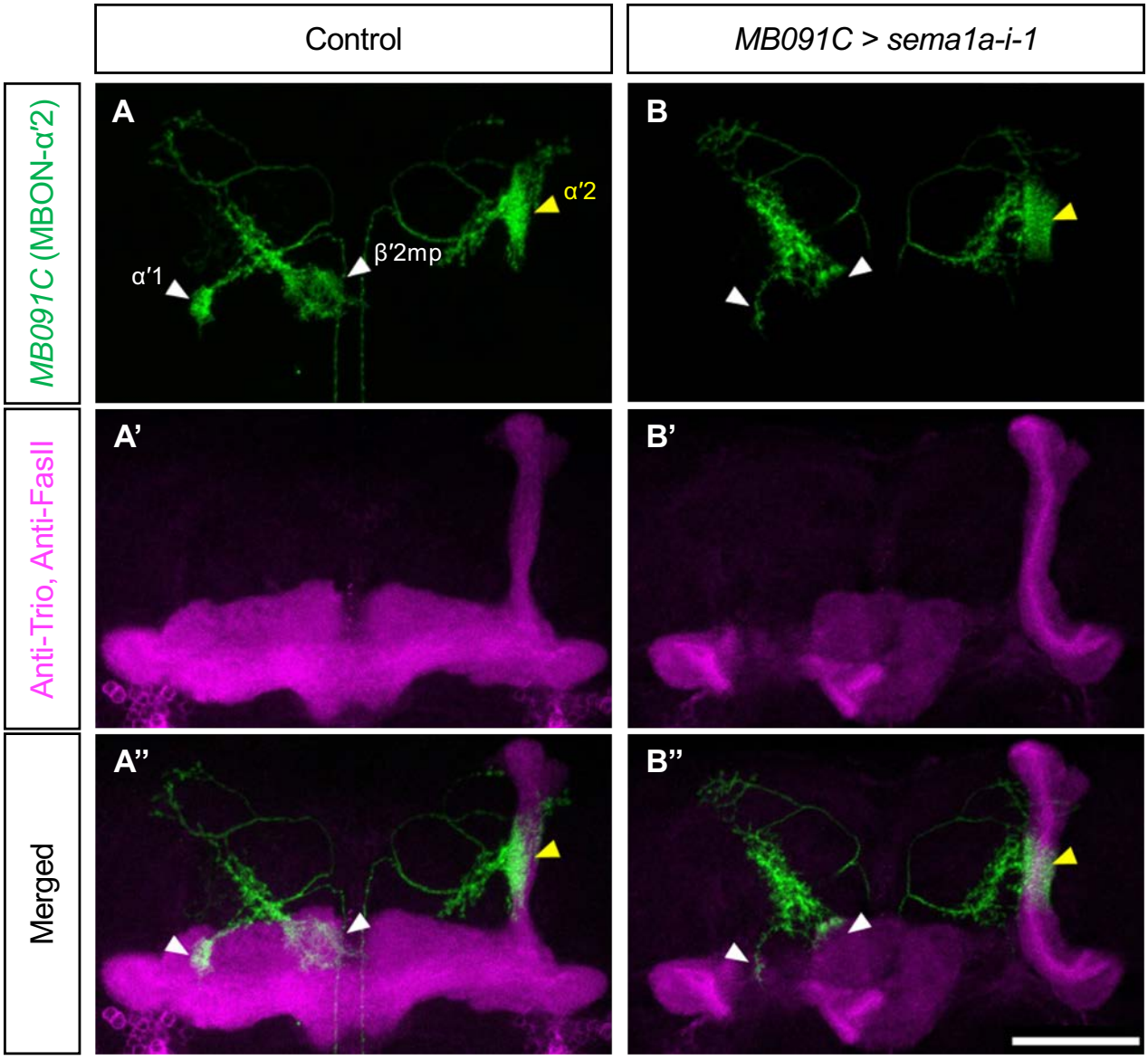
Control
MB091C > sema1a-i-1
MB091C (MBON-α′2)
Anti-Trio, Anti-FasII
Merged
A
B
A’
B’
A”
B”
α′1
β′2mp
α′2

Figure 8

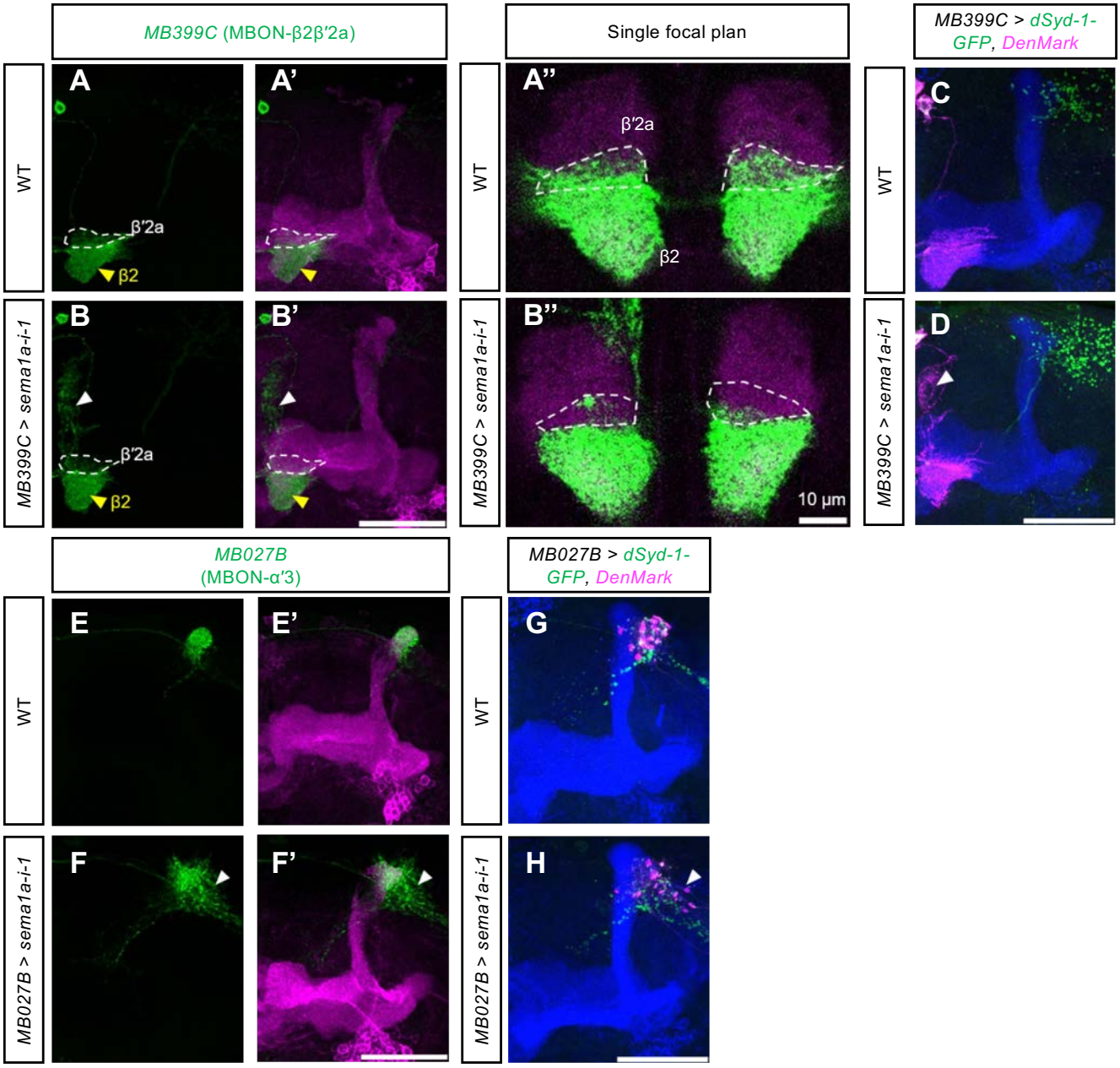
MB399C (MBON-β2β′2a)
Single focal plan
MB399C > dSyd-1-GFP, DenMark
WT
MB399C > sema1a-i-1
A
A'
A''
B
B'
B''
C
D
β′2a
β2
10 µm
MB027B (MBON-α′3)
MB027B > dSyd-1-GFP, DenMark
MB027B > sema1a-i-1
E
E'
F
F'
G
H

Figure 9

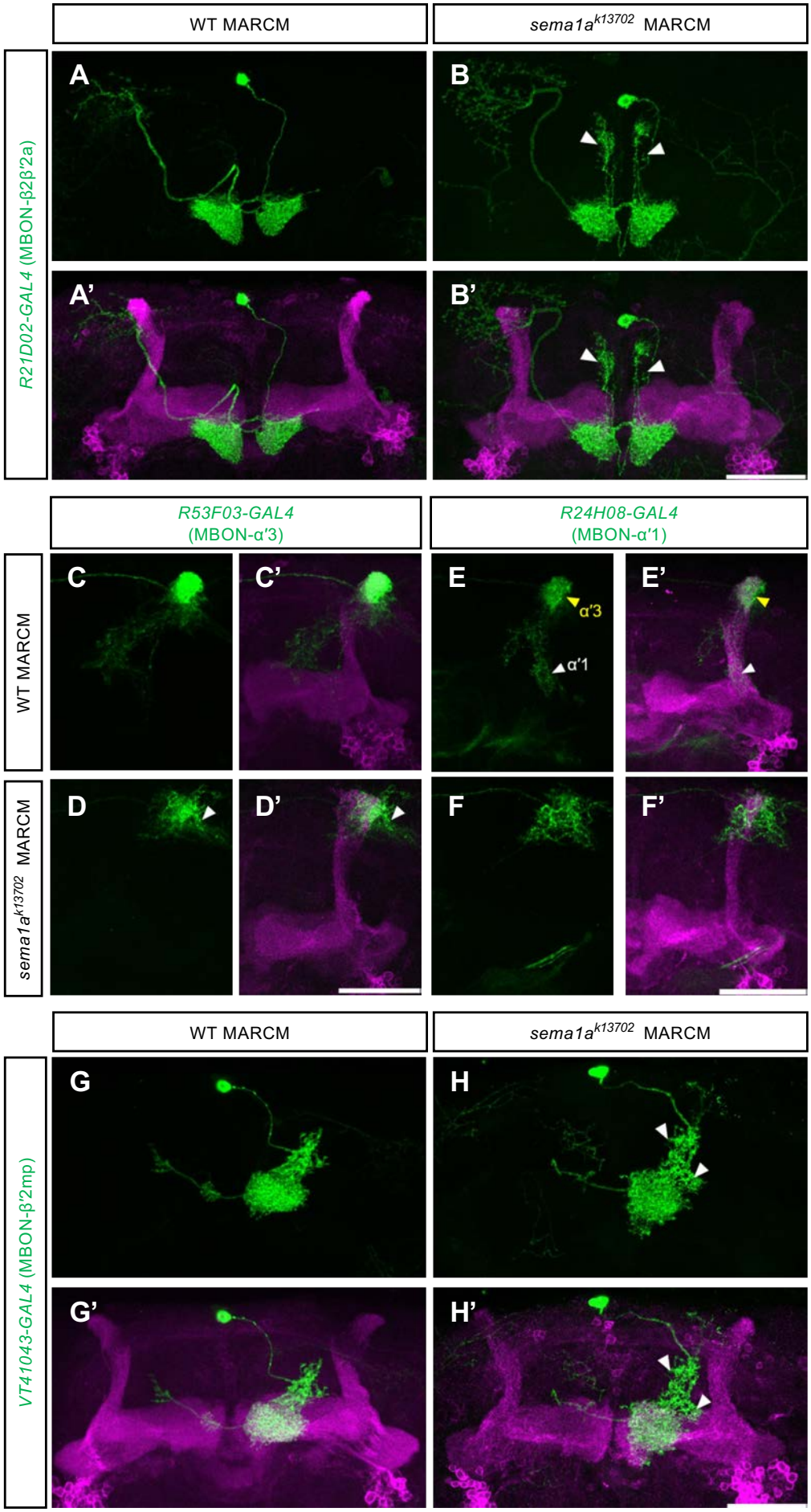
WT MARCM
sema1a^{k13702} MARCM
R21D02-GAL4 (MBON-β2β′2a)
A
B
A′
B′
R53F03-GAL4
(MBON-α′3)
R24H08-GAL4
(MBON-α′1)
WT MARCM
sema1a^{k13702} MARCM
C
C′
E
E′
α′3
α′1
D
D′
F
F′
WT MARCM
sema1a^{k13702} MARCM
VT41043-GAL4 (MBON-β′2mp)
G
H
G′
H′

Figure 10

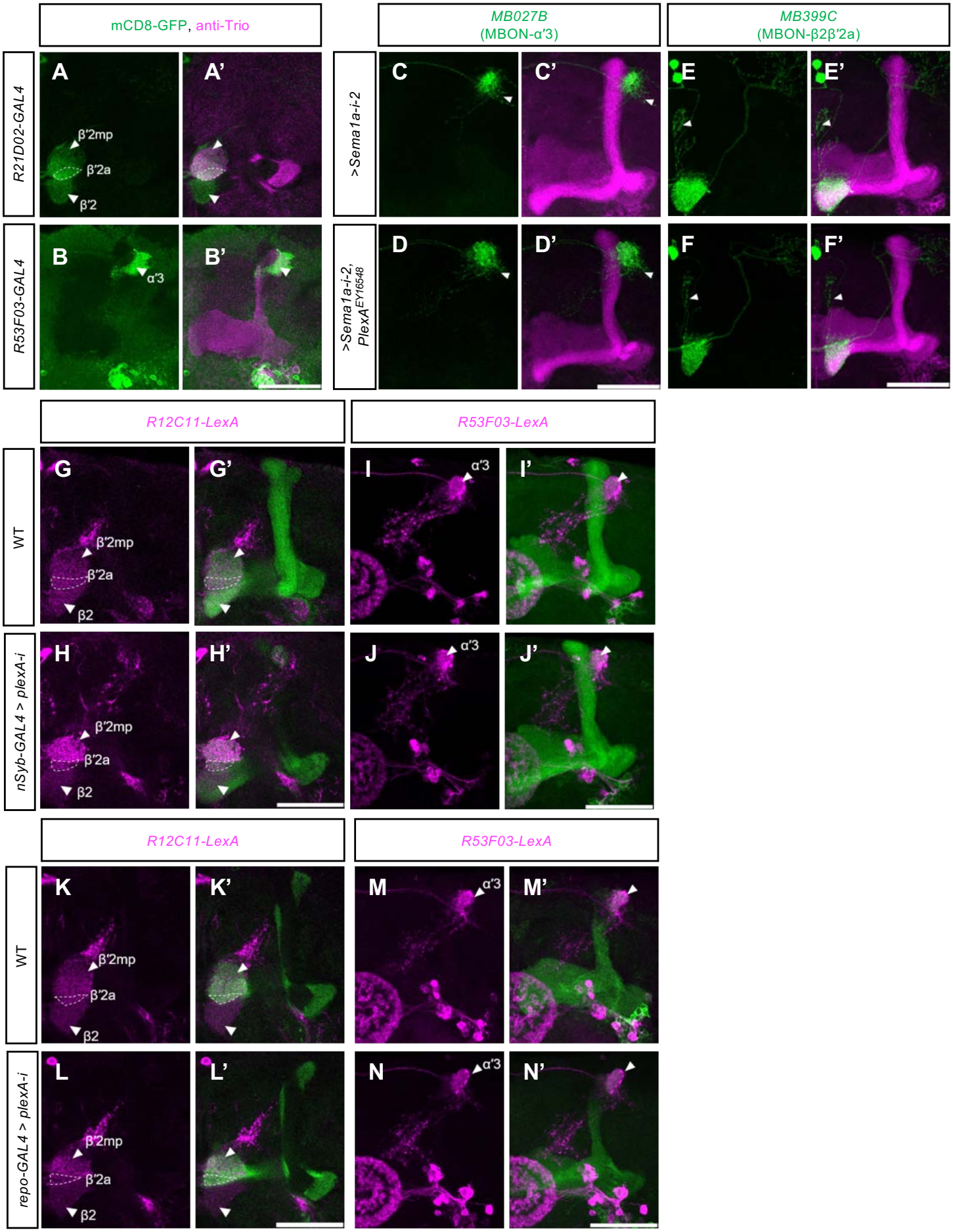
mCD8-GFP, anti-Trio
MB027B
(MBON-α′3)
MB399C
(MBON-β2β′2a)
R21D02-GAL4
R53F03-GAL4
>Sema1a-i-2
>Sema1a-i-2, PlexA^EY16548
A
A'
B
B'
C
C'
D
D'
E
E'
F
F'
β′2mp
β′2a
β′2
α′3
R12C11-LexA
R53F03-LexA
WT
nSyb-GAL4 > plexA-i
repo-GAL4 > plexA-i
G
G'
H
H'
I
I'
J
J'
K
K'
L
L'
M
M'
N
N'
β2